Engineering Analysis with Boundary Elements 85 (2017) 70–86

Contents lists available at ScienceDirect

Engineering Analysis with Boundary Elements

journal homepage: www.elsevier.com/locate/enganabound

# Analytical derivation and numerical experiment of degenerate scale by using the degenerate kernel of the bipolar coordinates

Jeng-Tzong Chen[a,b,*], Shing-Kai Kao[a], Jia-Wei Lee[c]

[a] Department of Harbor and River Engineering, National Taiwan Ocean University, Keelung, Taiwan
[b] Department of Mechanical and Mechatronic Engineering, National Taiwan Ocean University, Keelung, Taiwan
[c] Department of Civil Engineering, Tamkang University, New Taipei City, Taiwan

ARTICLE INFO

*Keywords:*
Degenerate scale
Degenerate kernel
Bipolar coordinates
Eccentric annulus

ABSTRACT

Degenerate scales of an eccentric annulus and an infinite plane with two identical circular holes in the boundary integral equation method (BIEM) are analytically derived and numerically implemented in this paper. To analytically study the degenerate scale of the BIE, the closed-form fundamental solution of the two-dimensional Laplace equation, $\ln r$, is expanded by a degenerate (separate) kernel in terms of the bipolar coordinates. It is proved that unit radius of the outer circle dominates the degenerate scale of eccentric annulus. An analytical formula of degenerate scale for the infinite plane with two identical circular boundaries was also derived at the first time. In addition, null fields of the domain and complementary domain for the ordinary and degenerate scales are both shown, respectively. Finally, comparison with available results and the BEM data are well done.



## 1. Introduction

Boundary integral equation method (BIEM)/boundary element method (BEM) is efficient and accurate for solving two-dimensional problems governed by the Laplace equation, the Navier equation or the biharmonic equation. However, the Dirichlet type problem of a special domain may yield a nonunique solution once the single-layer kernel is used. This special size is called the degenerate scale. The degenerate scale is related to Gamma contour [1], logarithmic capacity [2], critical value [3] and transfinite boundary [4] but the concepts are the same. Therefore, how to predict the degenerate scale appearing in the BIEM/BEM is very important and is not trivial in the development of the BEM. For this reason, many researchers paid attention to this issue in recent years [5–7].

When the real size is at a degenerate scale in the BIEM/BEM implementation, it results in a singular influence matrix due to a weakly singular kernel (U). In other words, the occurrence of the degenerate scale is inherent in the integral equation. Hence, the degenerate scale is not physically realizable but is mathematically interpretable. From the viewpoint of mathematics, there are two ways to understand the degenerate scale. One is the non-uniqueness solution in the BIEM/BEM. The other is the unit logarithmic capacity corresponding to the conformal radius in the complex analysis [8]. When the logarithmic capacity is equal to 1, the corresponding scale is a degenerate one. There were analytical formulae of the logarithmic capacity for the fourteen geometry shapes presented by Landkof [9]. Dijkstra [10] numerically examined the value of the degenerate scale for some geometry shapes [6] by using the BEM. However, the derivation of the analytical formulae was not given in Landkof's book [9]. Later, Rumely [2] employed the conformal mapping to analytically derive the logarithmic capacity for many shapes such as the circle, the ellipse and the disjoint circles. However, the relation between the logarithmic capacity and the degenerate scale was not addressed in their books [2,9]. Until 2013, Kuo et al. [11] employed the Riemann conformal mapping to link the unit logarithmic capacity and the degenerate scale. One way to understand the degenerate scale which results in the non-uniqueness solution in the BIEM/BEM is the range deficiency of the integral operator of a weakly singular kernel, $\ln r$.

Chen et al. [12] employed the degenerate kernel and the circulant to analytically study the degenerate scale of circular and annular geometries in the continuous and discrete systems, respectively. Later, the numerical demonstration was achieved in an eccentric annulus case by Chen and Shen [13]. But the analytical expressions were not provided. An annular region has also been considered for the harmonic equation by He et al. [14], Liu and Lean [15]. Possible degenerate scales were studied in both continuous and discrete systems. However, the

* Corresponding author at: Department of Harbor and River Engineering, National Taiwan Ocean University, Keelung, Taiwan.
*E-mail address:* jtchen@mail.ntou.edu.tw (J.-T. Chen).

http://dx.doi.org/10.1016/j.enganabound.2017.08.006
Received 2 December 2016; Received in revised form 3 August 2017; Accepted 3 August 2017
Available online 10 October 2017
0955-7997/

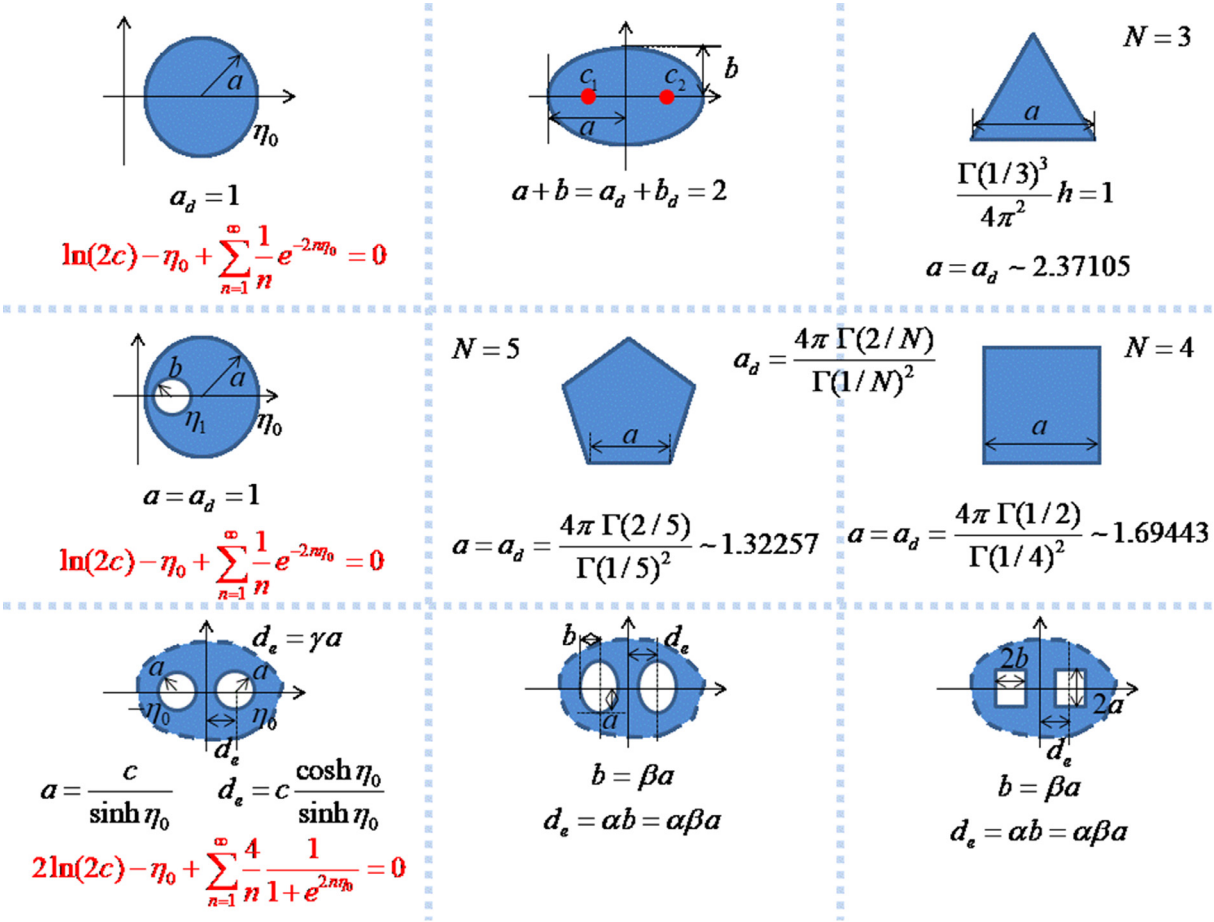


**Fig. 1.** Degenerate scale of several shapes of domain.

circulant property fails in the non-circular or non-annular case. Therefore, Chen et al. [16] used the BEM to numerically investigate the degenerate scale of an ellipse and found that there exist two degenerate scales in the plane elasticity. Related works were done by Chen and his coworkers [17–19]. Besides, Chen et al. [20] also extended the BIEM/BEM to study the degenerate scale for a circular thin plate (biharmonic equation). Regarding the multiply-connected domain, it is found that the degenerate scale depends on the outer boundary contour [21,22]. Chen and Shen [13] also numerically demonstrated that the degenerate scale of an eccentric annulus depends on the unit radius of the outer circle. However, no analytical proof was done to the best of authors' knowledge. Here, we would present it by using the bipolar coordinates for an eccentric annulus.

Corfdir and Bonnet [23] studied the Laplace problem of degenerate scale for a half-plane domain. In their paper, they claimed that the degenerate scale depends on the type of the boundary condition on the line bounding the half-plane. The degenerate scale only occurs for the Neumann boundary condition. On the contrary, it does not appear for the Dirichlet type. The half-plane problem can be transformed into an infinite-plane problem with the symmetric or the anti-symmetric Dirichlet boundary condition. Later, Chen [24] employed a null-field BIEM to study the same problem. Numerical results [24] also support the finding in [23]. However, from the viewpoint of using the indirect BIEM/BEM, the influence matrices constructed by the weakly singular kernel ($\ln r$) for those two infinite-plane problems are the same. For two holes in the infinite plane, they may have the same degenerate scale no matter that it is symmetric or anti-symmetric Dirichlet boundary conditions since the influence matrices are the same. In those two papers [23, 24], both of them employed the image method to construct the corresponding Green's function. The boundary condition on the line bounding the half-plane can be satisfied in advance by using the Green's function in their BEM formulations. In this way, the degenerate scale is free for the Dirichlet condition on the line bounding the half-plane. In this paper, we adopted the usual kernel ($\ln r$) in our BEM formulation for all kinds of boundary conditions. This is the reason why we will examine the present result and those of the two papers. This finding also verifies again that the degenerate scale depends on the kernel function in the BEM/BIEM.

In addition, the null and nonzero fields for ordinary and degenerate scales are also the main focus of the present study. Chen et al. [25] analytically studied the field of both interior and exterior domains for an elliptical case. They found that the trivial boundary potential may result in a nontrivial boundary flux when the geometric size is at a degenerate scale. It means that the fields inside and outside the domain are null and nonzero for a domain at the degenerate scale, respectively. This phenomenon is not physically realizable and is opposite to the phenomenon of ordinary scale. In 2012, Chen et al. [26] employed the null-field BIEM in conjunction with the degenerate kernel to revisit the same problem. The same result was obtained. Later, Kuo et al. [6] used the BEM to numerically examine the null and nonzero fields for regular N-gon domains including right triangle, square, regular 5-gon and regular 6-gon. All numerical phenomena about degenerate scales obtained by the BEM agreed with the analytical prediction. Furthermore, true and spurious eigensolutions also have similar behavior of null and nonzero modes. Chen et al. [27] employed both BEM and the null-field BIEM to numerically demonstrate and analytically examine the null and nonzero modes for circular, elliptical, annular and confocal elliptical membranes. Not only true eigenmodes but also spurious eigenmodes were addressed. However, all the studies of degenerate scale and spurious eigenmodes

were focused on simply-connected domains. In this paper, we will extend to multiply-connected and infinite domains.

For the nine familiar shapes in Fig. 1, we had analytically studied the former six shapes (Circle [12], ellipse [25,26], eccentric annulus [13], regular N-gons [6]). In this paper, the degenerate scale of an infinite plane containing two identical circular holes is analytically derived by using the null-field BIEM. In our approach, we employ the bipolar coordinates to naturally describe the geometry of the mentioned problem. The closed-form kernel functions and boundary densities are expanded in terms of degenerate kernels and the eigenfunction expansion, respectively. In this way, all boundary contour integrals are exactly obtained. Therefore, the analytical derivation of the degenerate scale can be achieved. In addition, a special case of a circular domain and an eccentric annulus are also revisited by using the bipolar coordinates. Regarding the above three cases, it is found that influence matrices of the BEM may be singular for a certain scale as shown in the numerical evidence of Fig. 2. Finally, we also analytically derive and numerically verify the nonzero field in the domain and the null field in the complementary domain for the ordinary scale of these cases. It is found that analytical solutions match well numerical results obtained by using the BEM. For the special geometry, the infinite plane containing two rectangles or two ellipses, the BEM is also implemented to compare with available results in order to numerically demonstrate the existence of degenerate scale for an infinite plane with two arbitrary cavities.

## 2. Analytical derivation of the degenerate scale by using the bipolar coordinates

A degenerate scale is a well-known phenomenon for researchers and engineers using the BEM/BIEM. It is a certain size of the domain which results in non-uniqueness solutions in the boundary integral equation (BIE) for solving interior two-dimensional Laplace problems subject to the specified Dirichlet boundary condition. The Laplace equation subject to the Dirichlet boundary condition is given below:

$$\nabla^2 u(\mathbf{x}) = 0, \ \mathbf{x} \in D, \tag{1}$$

$$u(\mathbf{x}) = \bar{u}(\mathbf{x}), \ \mathbf{x} \in B, \tag{2}$$

where $D$ is the domain bounded by the boundary $B$ and $\bar{u}(\mathbf{x})$ is the specified Dirichlet condition. The boundary integral formulation for the Laplace equation can be derived from Green's third identity,

$$2\pi u(\mathbf{x}) = \int_B T(\mathbf{s},\mathbf{x}) u(\mathbf{s}) dB(\mathbf{s}) - \int_B U(\mathbf{s},\mathbf{x}) t(\mathbf{s}) dB(\mathbf{s}), \ \mathbf{x} \in D, \tag{3}$$

for the domain point, where $\mathbf{s}$ and $\mathbf{x}$ are the source and field points, respectively, $t(\mathbf{s}) = \frac{\partial u(\mathbf{s})}{\partial \mathbf{n_s}}$, in which $\mathbf{n_s}$ denotes the unit outward normal vector at the source point $\mathbf{s}$, and $U(\mathbf{s}, \mathbf{x})$ is the fundamental solution which satisfies

$$\nabla^2 U(\mathbf{s},\mathbf{x}) = 2\pi\delta(\mathbf{x}-\mathbf{s}), \tag{4}$$

where $\delta(\mathbf{x}-\mathbf{s})$ denotes the Dirac-delta function. The fundamental solution can be obtained as follows:

$$U(\mathbf{s},\mathbf{x}) = \ln|\mathbf{s}-\mathbf{x}| = \ln r, \tag{5}$$

where $r$ is the distance between $\mathbf{s}$ and $\mathbf{x}$, and the $T(\mathbf{s}, \mathbf{x})$ kernel function is defined by

$$T(\mathbf{s},\mathbf{x}) = \frac{\partial U(\mathbf{s},\mathbf{x})}{\partial \mathbf{n_s}}. \tag{6}$$

Eq. (3) is also called the direct BIE. If the two kernel functions were expressed in terms of proper degenerate kernels, then the null-field boundary integral equation would be

$$0 = \int_B T(\mathbf{s},\mathbf{x}) u(\mathbf{s}) dB(\mathbf{s}) - \int_B U(\mathbf{s},\mathbf{x}) t(\mathbf{s}) dB(\mathbf{s}), \ \mathbf{x} \in D^c \cup B, \tag{7}$$

where $D^c$ is the complementary domain. Using the degenerate kernel to represent the closed-form fundamental solution, the discontinuous behavior of potential due to $T(\mathbf{s}, \mathbf{x})$ across the boundary can be expressed

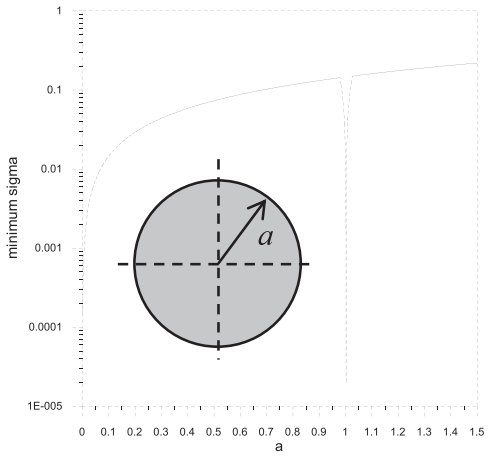


(a) A circle (degenerate scale, $a$=1)

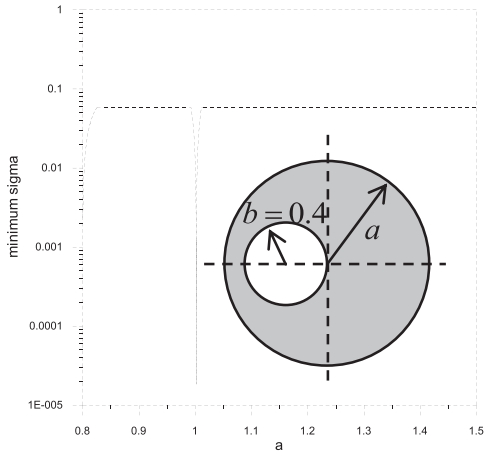


(b) An eccentric annulus (degenerate scale, $a$=1)

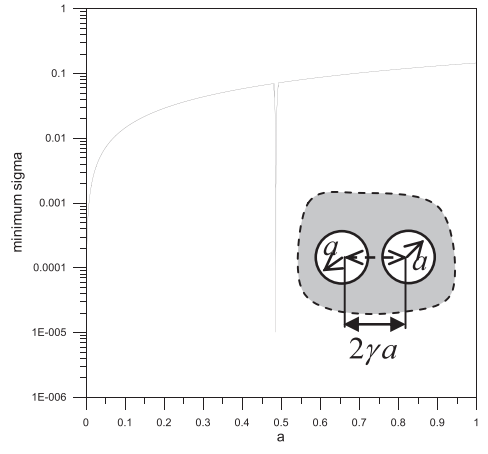


(c) An infinite plane with two identical circular holes (degenerate scale, $a = 0.48513, \gamma = 2$)

**Fig. 2.** Numerical evidences for the degenerate scale of three cases in BEM. (a) A circle (degenerate scale, $a=1$). (b) An eccentric annulus (degenerate scale, $a=1$). (c) An infinite plane with two identical circular holes (degenerate scale, $a=0.48513$, $\gamma=2$).

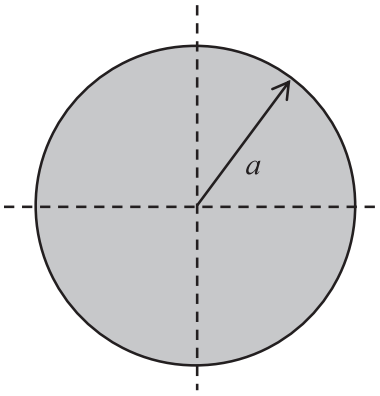


(a) A circle

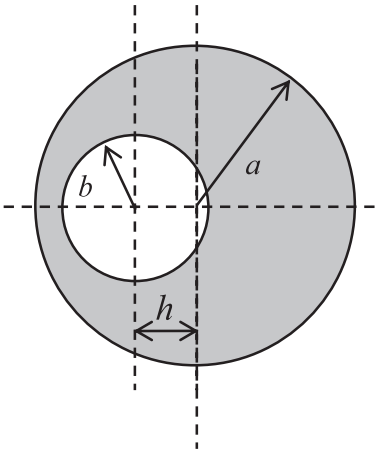


(b) An eccentric annulus

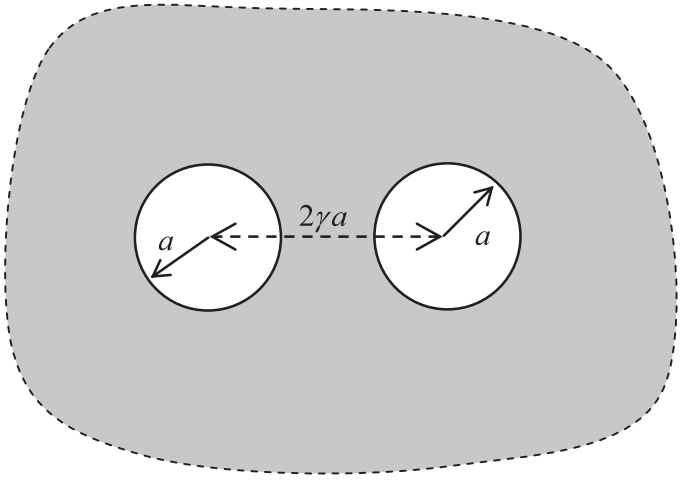


(c) An infinite plane with two identical circular holes

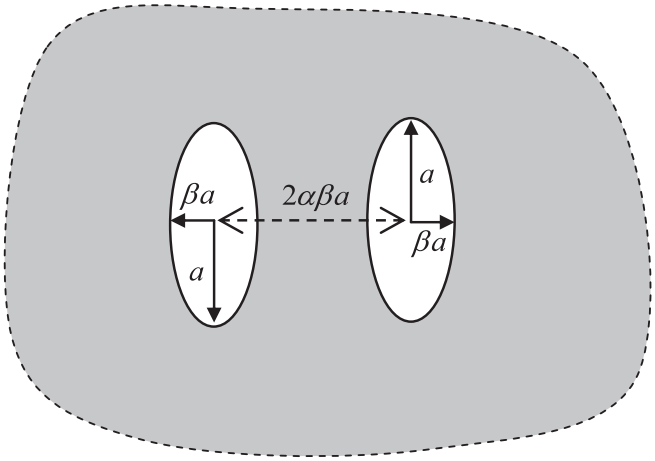


(d) An infinite plane with two identical elliptical holes

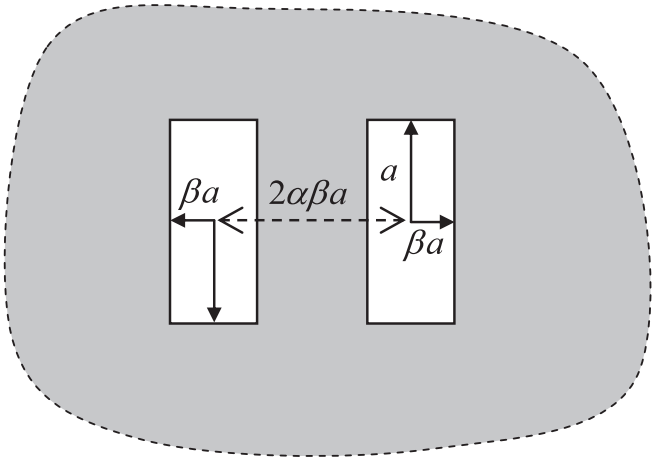


(e) An infinite plane with two identical rectangular holes

**Fig. 3.** Sketch of three analytical cases and two numerical cases.

clearly by each side. Therefore, the Cauchy principal value and bump contour [28] are not used and no free term is required in Eq. (7). The influence matrices for boundary points obtained by using both the domain point BIE and null-field BIE are the same [29]. Here, three cases, a circular domain, an eccentric annulus and an infinite domain with two identical circular holes are considered as shown in Fig. 3(a)–(c). In order to analytically derive the degenerate scale of a problem containing two circular boundaries, we employ the kernel function in the bipolar coordinates ($\eta$, $\xi$). The closed-form fundamental solution, $\ln r$, is expanded into the degenerate form by separating the source point and the field

point as shown below:

$$U(\mathbf{s},\mathbf{x})=\begin{cases}\ln(2c)-\eta_s-\sum\limits_{n=1}^{\infty}\frac{1}{n}\left[e^{-n(\eta_x-\eta_s)}\cos\left[n(\xi_x-\xi_s)\right]\right.\\ \quad\left.-e^{-n\eta_x}\cos(n\xi_x)-e^{-n\eta_s}\cos(n\xi_s)\right],\quad \eta_x\geq\eta_s\geq 0,\\ \ln(2c)-\eta_x-\sum\limits_{n=1}^{\infty}\frac{1}{n}\left[e^{-n(\eta_s-\eta_x)}\cos\left[n(\xi_x-\xi_s)\right]-e^{-n\eta_x}\cos(n\xi_x)\right.\\ \quad\left.-e^{-n\eta_s}\cos(n\xi_s)\right],\quad \eta_s>\eta_x>0,\\ \ln(2c)-\sum\limits_{n=1}^{\infty}\frac{1}{n}\left[e^{-n(\eta_s-\eta_x)}\cos\left[n(\xi_x-\xi_s)\right]-e^{n\eta_x}\cos(n\xi_x)\right.\\ \quad\left.-e^{-n\eta_s}\cos(n\xi_s)\right],\quad \eta_s>0>\eta_x,\end{cases}\tag{8}$$

where $\eta_s\geq 0$, $\mathbf{x}=(\eta_x,\xi_x)$, $\mathbf{s}=(\eta_s,\xi_s)$, $c$ is the half distance between the two foci of the bipolar coordinates and the relationship between Cartesian coordinates $(x_1,x_2)$ and the bipolar coordinates $(\eta_x,\xi_x)$ are

$$x_1=c\frac{\sinh\eta_x}{\cosh\eta_x-\cos\xi_x},\tag{9}$$

$$x_2=c\frac{\sin\xi_x}{\cosh\eta_x-\cos\xi_x}.\tag{10}$$

If $\eta_s<0$, the kernel function is similarly expanded as:

$$U(\mathbf{s},\mathbf{x})=\begin{cases}\ln(2c)+\eta_s-\sum\limits_{n=1}^{\infty}\frac{1}{n}\left[e^{-n(\eta_s-\eta_x)}\cos\left[n(\xi_x-\xi_s)\right]\right.\\ \quad\left.-e^{n\eta_x}\cos(n\xi_x)-e^{n\eta_s}\cos(n\xi_s)\right],\quad \eta_x\leq\eta_s<0,\\ \ln(2c)\ +\ \eta_x\ -\sum\limits_{n=1}^{\infty}\frac{1}{n}\left[e^{-n(\eta_x-\eta_s)}\cos\left[n(\xi_x-\xi_s)\right]\right.\\ \quad\left.-e^{n\eta_x}\cos(n\xi_x)-e^{n\eta_s}\cos(n\xi_s)\right],\quad \eta_s<\eta_x<0,\\ \ln(2c)-\sum\limits_{n=1}^{\infty}\frac{1}{n}\left[e^{-n(\eta_x-\eta_s)}\cos\left[n(\xi_x-\xi_s)\right]\right.\\ \quad\left.-e^{-n\eta_x}\cos(n\xi_x)-e^{n\eta_s}\cos(n\xi_s)\right],\quad \eta_s<0<\eta_x.\end{cases}\tag{11}$$

To verify the validity of Eqs. (8) and (11), the contour plots of the closed-form fundamental solution and the degenerate kernel are shown in Table 1. To fully employ the degenerate kernel in the bipolar coordinates, a circular case, an eccentric annulus and an infinite plane with two identical circular holes are considered. In the following three subsections, we individually investigate the degenerate scale of these three cases.

### 2.1. Revisit of the degenerate scale of a circular domain by using the bipolar coordinates

First, we revisit the degenerate scale of a circular domain by using the degenerate kernel in terms of the bipolar coordinates instead of the polar coordinates [12]. The specified Dirichlet boundary condition along the boundary ($\eta_s=\eta_0$) can be expanded by using the Fourier series,

$$\bar{u}(\mathbf{s})=p_0+\sum_{n=1}^{\infty}p_n\cos(n\xi_s)+\sum_{n=1}^{\infty}q_n\sin(n\xi_s),\quad \mathbf{s}\in B\ and\ 0\leq\xi_s\leq 2\pi,\ \eta_s=\eta_0=\text{const.},\tag{12}$$

where $\mathbf{s}=(\eta_s,\xi_s)$, coefficients of Fourier series, $p_0$, $p_n$ and $q_n$ are given from the Dirichlet B.C. The unknown boundary flux density of normal derivative, $t(\mathbf{s})$, is expressed by

$$t(\mathbf{s})=-\frac{\cosh\eta_0-\cos\xi_s}{c}\left[a_0+\sum_{n=1}^{\infty}a_n\cos(n\xi_s)+\sum_{n=1}^{\infty}b_n\sin(n\xi_s)\right],\quad \mathbf{s}\in B\text{ and }0\leq\xi_s\leq 2\pi,\tag{13}$$

since $\partial(\cdot)/\partial\mathbf{n}_s=-\frac{\cosh\eta_s-\cos\xi_s}{c}\partial(\cdot)/\partial\eta_s$. In Eq. (13), $a_0$, $a_n$ *and* $b_n$ are the unknown coefficients of Fourier series to be determined. For the boundary contour, we have

$$dB(\mathbf{s})=\frac{c}{\cosh(\eta_s)-\cos(\xi_s)}d\xi_s.\tag{14}$$

Based on Eqs. (6) and (14), substitution of $\eta_x=\eta_0$, Eqs. (8), (12) and (13) into Eq. (7) yields

$$\begin{aligned}&2\pi\left(\ln(2c)-\eta_0\right)a_0-\sum_{n=1}^{\infty}\frac{\pi}{n}\cos(n\xi_x)a_n-\sum_{n=1}^{\infty}\frac{\pi}{n}\sin(n\xi_x)b_n\\&+\sum_{n=1}^{\infty}\frac{2\pi}{n}e^{-n\eta_0}\cos(n\xi_x)a_0+\sum_{n=1}^{\infty}\frac{\pi}{n}e^{-n\eta_0}a_n\\&=2\pi\left(p_0+\sum_{n=1}^{\infty}e^{-n\eta_0}p_n\right)+\pi\sum_{n=1}^{\infty}p_n\cos(n\xi_x)\\&+\pi\sum_{n=1}^{\infty}q_n\sin(n\xi_x),\quad \mathbf{x}\in B\text{ and }0\leq\xi_x\leq 2\pi.\end{aligned}\tag{15}$$

By comparing with the coefficient of the Fourier sine base in Eq. (15), we have

$$b_n=-nq_n.\tag{16}$$

However, the coefficients, $a_0$ and $a_n$ of cosine terms are coupled as shown below:

$$\begin{aligned}&2\left(\ln(2c)-\eta_0\right)a_0+\sum_{n=1}^{\infty}\frac{1}{n}e^{-n\eta_0}a_n\\&=2\left(p_0+\sum_{n=1}^{\infty}e^{-n\eta_0}p_n\right),\ \text{for the constant term,}\end{aligned}\tag{17}$$

$$\frac{2}{n}e^{-n\eta_0}a_0-\frac{1}{n}a_n=p_n,\ \text{for the}\ \cos(n\xi_x)\,\text{term}\tag{18}$$

After decoupling $a_0$ and $a_n$ in Eqs. (17) and (18), we have

$$\left(\ln(2c)-\eta_0+\sum_{n=1}^{\infty}\frac{1}{n}e^{-2n\eta_0}\right)a_0=p_0-\frac{3}{2}\sum_{n=1}^{\infty}e^{-n\eta_0}p_n.\tag{19}$$

If the coefficient of $a_0$ in Eq. (19) is equal to zero, i.e.

$$\ln(2c)-\eta_0+\sum_{n=1}^{\infty}\frac{1}{n}e^{-2n\eta_0}=0,\tag{20}$$

then $a_0$ cannot be determined. The value of $\eta_0$ satisfying Eq. (20) denoted by $\eta_d$ yields the degenerate scale. Based on the addition theorem of ln function [30], we have

$$\ln(a-b)=\ln a-\sum_{n=1}^{\infty}\frac{1}{n}\left(\frac{b}{a}\right)^n,\quad \left|\frac{b}{a}\right|<1.\tag{21}$$

By setting $a=e^{\eta_d}$ and $b=e^{-\eta_d}$ in Eq. (21), Eq. (20) is simplified to

$$\ln(2c)-\ln\left(e^{\eta_d}-e^{-\eta_d}\right)=0,\tag{22}$$

i.e.

$$\frac{2c}{e^{\eta_d}-e^{-\eta_d}}=1.\tag{23}$$

The radius of the circle, $a$, in the bipolar coordinates is expressed by

$$a=\frac{c}{\sinh\eta_0},\ \eta_0>0.\tag{24}$$

Eq. (23) in conjunction with Eq. (24) proves that the degenerate scale of a circular domain is $a=a_d=c/\sinh\eta_d=1$ as shown in Fig. 1. This result matches well that of a circle by using the degenerate kernel of the polar coordinates [12]. In the BEM implementation, the influence matrix constructed by using the $U(\mathbf{s},\mathbf{x})$ kernel may be singular when the radius is one (degenerate scale) as shown in Fig. 2(a).

**Table 1**
Sketch of contour plots of the closed-form fundamental solution and the degenerate kernel.

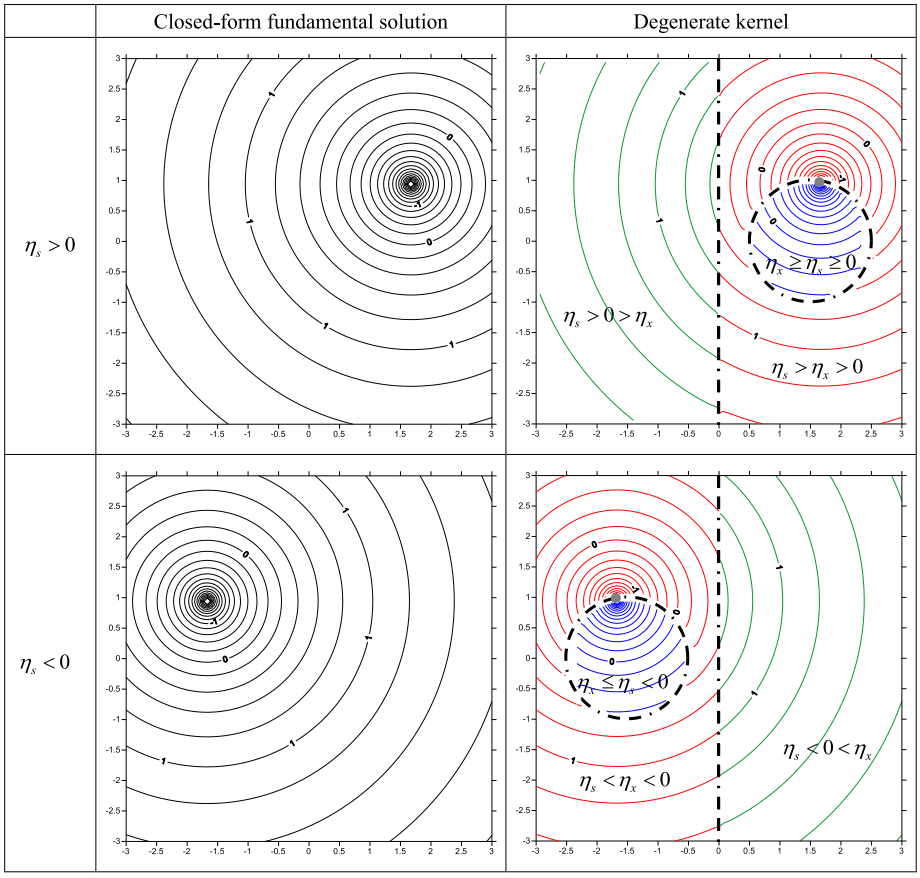


### 2.2. Analytical derivation of the degenerate scale of an eccentric annulus by using the bipolar coordinates

Similarly, the given and unknown boundary data of an eccentric annulus are expressed by

$$u_0(\mathbf{s}) = p_0^{(0)} + \sum_{n=1}^{\infty} p_n^{(0)} \cos(n\xi_s) + \sum_{n=1}^{\infty} q_n^{(0)} \sin(n\xi_s), \ \mathbf{s} \in B_0 \text{ and } 0 \leq \xi_s \leq 2\pi, \tag{25}$$

$$u_1(\mathbf{s}) = p_0^{(1)} + \sum_{n=1}^{\infty} p_n^{(1)} \cos(n\xi_s) + \sum_{n=1}^{\infty} q_n^{(1)} \sin(n\xi_s), \ \mathbf{s} \in B_1 \text{ and } 0 \leq \xi_s \leq 2\pi, \tag{26}$$

and

$$t_0(\mathbf{s}) = -\frac{\cosh\eta_0 - \cos\xi_s}{c}\left[a_0^{(0)} + \sum_{n=1}^{\infty} a_n^{(0)} \cos(n\xi_s) + \sum_{n=1}^{\infty} b_n^{(0)} \sin(n\xi_s)\right], \quad \mathbf{s} \in B_0 \text{ and } 0 \leq \xi_s \leq 2\pi, \tag{27}$$

$$t_1(\mathbf{s}) = -\frac{\cosh\eta_1 - \cos\xi_s}{c}\left[a_0^{(1)} + \sum_{n=1}^{\infty} a_n^{(1)} \cos(n\xi_s) + \sum_{n=1}^{\infty} b_n^{(1)} \sin(n\xi_s)\right], \quad \mathbf{s} \in B_1 \text{ and } 0 \leq \xi_s \leq 2\pi, \tag{28}$$

where the subscript '0' and '1' of $u$, $t$ and $B$ and the superscript '(0)' and '(1)' of the unknown coefficients of Fourier series, stand for the outer (0) and inner (1) circular boundaries of the domain, respectively.

According to Eqs. (6) and (14), substitution of Eqs. (8), (25)–(28) into Eq. (7) yields

$$\begin{aligned}
&2\pi\left(\ln(2c) - \eta_0\right)a_0^{(0)} - \sum_{n=1}^{\infty}\frac{\pi}{n}\cos(n\xi_x)a_n^{(0)} - \sum_{n=1}^{\infty}\frac{\pi}{n}\sin(n\xi_x)b_n^{(0)} \\
&+\sum_{n=1}^{\infty}\frac{2\pi}{n}e^{-n\eta_0}\cos(n\xi_x)a_0^{(0)} + \sum_{n=1}^{\infty}\frac{\pi}{n}e^{-n\eta_0}a_n^{(0)} \\
&+2\pi\left(\ln(2c) - \eta_0\right)a_0^{(1)} - \sum_{n=1}^{\infty}\frac{\pi}{n}e^{-n(\eta_1-\eta_0)}\cos(n\xi_x)a_n^{(1)} \\
&-\sum_{n=1}^{\infty}\frac{\pi}{n}e^{-n(\eta_1-\eta_0)}\sin(n\xi_x)b_n^{(1)} + \sum_{n=1}^{\infty}\frac{2\pi}{n}e^{-n\eta_0}\cos(n\xi_x)a_0^{(1)} + \sum_{n=1}^{\infty}\frac{\pi}{n}e^{-n\eta_1}a_n^{(1)} \\
&= 2\pi\left(\sum_{n=1}^{\infty}e^{-n\eta_0}p_n^{(0)} + \sum_{n=1}^{\infty}e^{-n\eta_1}p_n^{(1)}\right) - \pi\sum_{n=1}^{\infty}\left(p_n^{(0)} + e^{-n(\eta_0-\eta_1)}p_n^{(1)}\right)\cos(n\xi_x) \\
&-\pi\sum_{n=1}^{\infty}\left(q_n^{(0)} + e^{-n(\eta_0-\eta_1)}q_n^{(1)}\right)\sin(n\xi_x), \ \mathbf{x} \in B_0,
\end{aligned} \tag{29}$$

$$\begin{aligned}
&2\pi\left(\ln(2c) - \eta_0\right)a_0^{(0)} - \sum_{n=1}^{\infty}\frac{\pi}{n}e^{-n(\eta_1-\eta_0)}\cos(n\xi_x)a_n^{(0)} \\
&-\sum_{n=1}^{\infty}\frac{\pi}{n}e^{-n(\eta_1-\eta_0)}\sin(n\xi_x)b_n^{(0)} + \sum_{n=1}^{\infty}\frac{2\pi}{n}e^{-n\eta_1}\cos(n\xi_x)a_0^{(0)} + \sum_{n=1}^{\infty}\frac{\pi}{n}e^{-n\eta_0}a_n^{(0)} \\
&+2\pi\left(\ln(2c) - \eta_1\right)a_0^{(1)} - \sum_{n=1}^{\infty}\frac{\pi}{n}\cos(n\xi_x)a_n^{(1)} \\
&-\sum_{n=1}^{\infty}\frac{\pi}{n}\sin(n\xi_x)b_n^{(1)} + \sum_{n=1}^{\infty}\frac{2\pi}{n}e^{-n\eta_1}\cos(n\xi_x)a_0^{(1)} + \sum_{n=1}^{\infty}\frac{\pi}{n}e^{-n\eta_1}a_n^{(1)}
\end{aligned}$$

$$= 2\pi\left(p_0^{(0)} + \sum_{n=1}^{\infty} e^{-n\eta_0} p_n^{(0)} + \sum_{n=1}^{\infty} e^{-n\eta_1} p_n^{(1)}\right)$$
$$+\pi \sum_{n=1}^{\infty} \left(e^{-n(\eta_1-\eta_0)} p_n^{(0)} - p_n^{(1)}\right) \cos(n\xi_x)$$
$$+\pi \sum_{n=1}^{\infty} \left(e^{-n(\eta_1-\eta_0)} q_n^{(0)} - q_n^{(1)}\right) \sin(n\xi_x), \ \mathbf{x} \in B_1, \tag{30}$$

by collocating on the outer and inner boundary points, respectively. After comparing with the coefficients in Eqs. (29) and (30), it is found that coefficients of sine, $b_n^{(0)}$ and $b_n^{(1)}$ are uncoupled with the coefficients of cosine, $a_0^{(0)}$, $a_n^{(0)}$, $a_0^{(1)}$ and $a_n^{(1)}$. The coefficients of sine could be determined in advance. After adding or subtracting the related equations of constant or cosine term, the coefficients satisfy

$$\left(\eta_1 - \eta_0\right) a_0^{(1)} = p_0^{(0)}, \tag{31}$$

$$2\left(\ln(2c) - \eta_0\right) a_0^{(0)} + \sum_{n=1}^{\infty} \frac{1}{n} e^{-n\eta_0} a_n^{(0)} + \left(2\ln(2c) - \eta_0 - \eta_1\right) a_0^{(1)}$$
$$+ \sum_{n=1}^{\infty} \frac{1}{n} e^{-n\eta_1} a_n^{(1)} = p_0^{(0)} + 2\left(\sum_{n=1}^{\infty} e^{-n\eta_0} p_n^{(0)} + \sum_{n=1}^{\infty} e^{-n\eta_1} p_n^{(1)}\right), \tag{32}$$

$$a_n^{(0)} - a_n^{(1)} = \frac{n}{1 - e^{-n(\eta_1-\eta_0)}} \left[\frac{2}{n}(e^{-n\eta_0} - e^{-n\eta_1})\left(a_0^{(0)} + a_0^{(1)}\right)\right.$$
$$\left. +\left(1 + e^{-n(\eta_1-\eta_0)}\right) p_n^{(0)} - \left(1 - e^{-n(\eta_1-\eta_0)}\right) p_n^{(1)}\right], \tag{33}$$

$$a_n^{(0)} + a_n^{(1)} = \frac{n}{1 + e^{-n(\eta_1-\eta_0)}} \left[\frac{2}{n}(e^{-n\eta_0} + e^{-n\eta_1})\left(a_0^{(0)} + a_0^{(1)}\right)\right.$$
$$\left. +\left(1 - e^{-n(\eta_1-\eta_0)}\right) p_n^{(0)} + \left(1 + e^{-n(\eta_1-\eta_0)}\right) p_n^{(1)}\right]. \tag{34}$$

Eqs. (33) and (34) yield

$$a_n^{(0)} = \left(\frac{n}{1 - e^{-2n(\eta_1-\eta_0)}}\right)\left[\frac{2}{n}\left(e^{-n\eta_0} - e^{-n\eta_1} e^{-n(\eta_1-\eta_0)}\right)\left(a_0^{(0)} + a_0^{(1)}\right)\right.$$
$$\left. +\left(1 + e^{-2n(\eta_1-\eta_0)}\right) p_n^{(0)}\right], \tag{35}$$

$$a_n^{(1)} = \left(\frac{n}{1 - e^{-2n(\eta_1-\eta_0)}}\right)\left[-2e^{-n(\eta_1-\eta_0)} p_n^{(0)} + \left(1 + e^{-2n(\eta_1-\eta_0)}\right) p_n^{(1)}\right]. \tag{36}$$

After substituting Eq. (35) into Eq. (32), Eq. (32) yields

$$2\left(\ln(2c) - \eta_0 + \sum_{n=1}^{\infty} \frac{1}{n} \frac{e^{-2n\eta_0} - e^{-n(\eta_1+\eta_0)} e^{-n(\eta_1-\eta_0)}}{1 - e^{-2n(\eta_1-\eta_0)}}\right) a_0^{(0)}$$
$$= p_0^{(0)} + 2\left(\sum_{n=1}^{\infty} e^{-n\eta_0} p_n^{(0)} + \sum_{n=1}^{\infty} e^{-n\eta_1} p_n^{(1)}\right) - \sum_{n=1}^{\infty} e^{-n\eta_0} \frac{1 + e^{-2n(\eta_1-\eta_0)}}{1 - e^{-2n(\eta_1-\eta_0)}} p_n^{(0)}$$
$$-\left(2\ln(2c) - \eta_0 - \eta_1 + \sum_{n=1}^{\infty} \frac{2}{n} \frac{e^{-2n\eta_0} - e^{-n(\eta_1+\eta_0)} e^{-n(\eta_1-\eta_0)}}{1 - e^{-2n(\eta_1-\eta_0)}}\right) a_0^{(1)}$$
$$- \sum_{n=1}^{\infty} \frac{1}{n} e^{-n\eta_1} a_n^{(1)}, \tag{37}$$

Based on Eq. (37) in conjunction with Eq. (31) for $a_0^{(1)}$ and Eq. (36) for $a_n^{(1)}$, we find that if the coefficient of $a_0^{(0)}$ is equal to zero, i.e.

$$\ln(2c) - \eta_0 + \sum_{n=1}^{\infty} \frac{1}{n} \frac{e^{-2n\eta_0} - e^{-n(\eta_1+\eta_0)} e^{-n(\eta_1-\eta_0)}}{1 - e^{-2n(\eta_1-\eta_0)}}$$
$$= \ln(2c) - \eta_0 + \sum_{n=1}^{\infty} \frac{1}{n} \frac{e^{-2n\eta_0}\left(1 - e^{-2n(\eta_1-\eta_0)}\right)}{1 - e^{-2n(\eta_1-\eta_0)}} = 0, \tag{38}$$

then $a_0^{(0)}$ cannot be determined. The parameter $\eta_0 = \eta_d$ satisfying Eq. (38) yields the degenerate scale. After the simplification, Eq. (38) is also reduced to the same as Eq. (20). Hence, the degenerate scale of the eccentric annulus depends on the radius of the outer circular boundary. The outer unit radius yields the degenerate scale. In the BEM implementation, a singular influence matrix occurs in the same size (degenerate scale) as shown in Fig. 2(b). These results agree with the finding [13].

### 2.3. Analytical derivation of the degenerate scale for the infinite plane with two identical circular holes

The degenerate scale of an infinite plane containing two identical circular holes is the main concern in this paper. The given and unknown boundary data of the two circular holes are expressed by

$$u_r(\mathbf{s}) = p_0^{(r)} + \sum_{n=1}^{\infty} p_n^{(r)} \cos(n\xi_s) + \sum_{n=1}^{\infty} q_n^{(r)} \sin(n\xi_s), \ \mathbf{s} \in B_r \text{ and } 0 \le \xi_s \le 2\pi, \tag{39}$$

$$u_l(\mathbf{s}) = p_0^{(l)} + \sum_{n=1}^{\infty} p_n^{(l)} \cos(n\xi_s) + \sum_{n=1}^{\infty} q_n^{(l)} \sin(n\xi_s), \ \mathbf{s} \in B_l \text{ and } 0 \le \xi_s \le 2\pi, \tag{40}$$

and

$$t_r(\mathbf{s}) = -\frac{\cosh\eta_0 - \cos\xi_s}{c}\left[a_0^{(r)} + \sum_{n=1}^{\infty} a_n^{(r)} \cos(n\xi_s) + \sum_{n=1}^{\infty} b_n^{(r)} \sin(n\xi_s)\right],$$
$$\mathbf{s} \in B_r \text{ and } 0 \le \xi_s \le 2\pi, \tag{41}$$

$$t_l(\mathbf{s}) = -\frac{\cosh\left(-\eta_0\right) - \cos\xi_s}{c}\left[a_0^{(l)} + \sum_{n=1}^{\infty} a_n^{(l)} \cos(n\xi_s) + \sum_{n=1}^{\infty} b_n^{(l)} \sin(n\xi_s)\right],$$
$$\mathbf{s} \in B_l \text{ and } 0 \le \xi_s \le 2\pi, \tag{42}$$

where the subscript '*r*' and '*l*' of *u*, *t* and *B* and the superscript '(*r*)' and '(*l*)' of the unknown coefficients of Fourier series, stand for the right hole and left one in the infinite plane, respectively. According to Eqs. (6) and (14), substitution of Eqs. (8,11,39–42) into Eq. (7) yields

$$2\pi\left(\ln(2c) - \eta_0\right) a_0^{(r)} - \sum_{n=1}^{\infty} \frac{\pi}{n} \cos(n\xi_x)\left(a_n^{(r)} - 2e^{-n\eta_0} a_0^{(r)}\right)$$
$$- \sum_{n=1}^{\infty} \frac{\pi}{n} \sin(n\xi_x) b_n^{(r)} + \sum_{n=1}^{\infty} \frac{\pi}{n} e^{-n\eta_0} a_n^{(r)}$$
$$+2\pi \ln(2c) a_0^{(l)} - \sum_{n=1}^{\infty} \frac{\pi}{n} \cos(n\xi_x)\left(e^{-2n\eta_0} a_n^{(l)} - 2e^{-n\eta_0} a_0^{(l)}\right)$$
$$- \sum_{n=1}^{\infty} \frac{\pi}{n} e^{-2n\eta_0} \sin(n\xi_x) b_n^{(l)} + \sum_{n=1}^{\infty} \frac{\pi}{n} e^{-n\eta_0} a_n^{(l)}$$
$$= \pi\left(2p_0^{(r)} + \sum_{n=1}^{\infty} e^{-n\eta_0} p_n^{(r)} + \sum_{n=1}^{\infty} e^{-n\eta_0} p_n^{(l)}\right)$$
$$+\pi \sum_{n=1}^{\infty} \left(p_n^{(r)} - e^{-2n\eta_0} p_n^{(l)}\right) \cos(n\xi_x)$$
$$+\pi \sum_{n=1}^{\infty} \left(q_n^{(r)} - e^{-2n\eta_0} q_n^{(l)}\right) \sin(n\xi_x), \ \mathbf{x} \in B_r, \tag{43}$$

$$2\pi \ln(2c) a_0^{(r)} - \sum_{n=1}^{\infty} \frac{\pi}{n} \cos(n\xi_x)\left(e^{-2n\eta_0} a_n^{(r)} - 2e^{-n\eta_0} a_0^{(r)}\right)$$
$$- \sum_{n=1}^{\infty} \frac{\pi}{n} e^{-2n\eta_0} \sin(n\xi_x) b_n^{(r)} + \sum_{n=1}^{\infty} \frac{\pi}{n} e^{-n\eta_0} a_n^{(r)}$$

$$+2\pi\left(\ln(2c)-\eta_0\right)a_0^{(l)}-\sum_{n=1}^{\infty}\frac{\pi}{n}\cos(n\xi_x)\left(a_n^{(l)}-2e^{-n\eta_0}a_0^{(l)}\right)$$
$$-\sum_{n=1}^{\infty}\frac{\pi}{n}\sin(n\xi_x)b_n^{(l)}+\sum_{n=1}^{\infty}\frac{\pi}{n}e^{-n\eta_0}a_n^{(l)}$$
$$=\pi\left(2p_0^{(l)}+\sum_{n=1}^{\infty}e^{-n\eta_0}p_n^{(r)}+\sum_{n=1}^{\infty}e^{-n\eta_0}p_n^{(l)}\right)$$
$$+\pi\sum_{n=1}^{\infty}\left(-e^{-2n\eta_0}p_n^{(r)}+p_n^{(l)}\right)\cos(n\xi_x)$$
$$+\pi\sum_{n=1}^{\infty}\left(-e^{-2n\eta_0}q_n^{(r)}+q_n^{(l)}\right)\sin(n\xi_x),\ \mathbf{x}\in B_l, \tag{44}$$

by collocating points on the right and left boundaries, respectively. After comparing with the coefficients of Fourier base in Eqs. (43) and (44), it is found that coefficients of sine are uncoupled and they could be determined. After adding or subtracting the related equations of constant or cosine term, the coefficients satisfy

$$\left(2\ln(2c)-\eta_0\right)\left(a_0^{(r)}+a_0^{(l)}\right)+\sum_{n=1}^{\infty}\frac{1}{n}e^{-n\eta_0}\left(a_n^{(r)}+a_n^{(l)}\right)=\left(p_0^{(r)}+p_0^{(l)}\right)$$
$$+\sum_{n=1}^{\infty}e^{-n\eta_0}\left(p_n^{(r)}+p_n^{(l)}\right), \tag{45}$$

$$\left(-\eta_0\right)\left(a_0^{(r)}-a_0^{(l)}\right)=p_0^{(r)}-p_0^{(l)}, \tag{46}$$

$$\frac{4}{n}e^{-n\eta_0}\left(a_0^{(r)}+a_0^{(l)}\right)-\frac{1}{n}\left(1+e^{-2n\eta_0}\right)\left(a_n^{(r)}+a_n^{(l)}\right)=\left(1-e^{-2n\eta_0}\right)\left(p_n^{(r)}+p_n^{(l)}\right), \tag{47}$$

$$\frac{1}{n}\left(1-e^{-2n\eta_0}\right)\left(a_n^{(r)}-a_n^{(l)}\right)=\left(1+e^{-2n\eta_0}\right)\left(p_n^{(r)}-p_n^{(l)}\right). \tag{48}$$

Eq. (47) can be rewritten as

$$\left(a_n^{(r)}+a_n^{(l)}\right)=\frac{4e^{-n\eta_0}}{1+e^{-2n\eta_0}}\left(a_0^{(r)}+a_0^{(l)}\right)-n\frac{1-e^{-2n\eta_0}}{1+e^{-2n\eta_0}}\left(p_n^{(r)}+p_n^{(l)}\right). \tag{49}$$

After substituting Eq. (49) into Eq. (45), Eq. (45) yields

$$\left(2\ln(2c)-\eta_0+\sum_{n=1}^{\infty}\frac{4}{n}\frac{e^{-2n\eta_0}}{1+e^{-2n\eta_0}}\right)\left(a_0^{(r)}+a_0^{(l)}\right)$$
$$=\left(p_0^{(r)}+p_0^{(l)}\right)+\sum_{n=1}^{\infty}\frac{2e^{-n\eta_0}}{1+e^{-2n\eta_0}}\left(p_n^{(r)}+p_n^{(l)}\right), \tag{50}$$

Based on Eqs. (46) and (50), $a_0^{(r)}$ and $a_0^{(l)}$ are expressed as

$$2\left(2\ln(2c)-\eta_0+\sum_{n=1}^{\infty}\frac{4}{n}\frac{e^{-2n\eta_0}}{1+e^{-2n\eta_0}}\right)a_0^{(r)}$$
$$=\left(p_0^{(r)}+p_0^{(l)}\right)+\sum_{n=1}^{\infty}\frac{2e^{-n\eta_0}}{1+e^{-2n\eta_0}}\left(p_n^{(r)}+p_n^{(l)}\right)$$
$$+\left(2\ln(2c)-\eta_0+\sum_{n=1}^{\infty}\frac{4}{n}\frac{e^{-2n\eta_0}}{1+e^{-2n\eta_0}}\right)\left(p_0^{(r)}-p_0^{(l)}\right)/(-\eta_0), \tag{51}$$

$$2\left(2\ln(2c)-\eta_0+\sum_{n=1}^{\infty}\frac{4}{n}\frac{e^{-2n\eta_0}}{1+e^{-2n\eta_0}}\right)a_0^{(l)}$$
$$=\left(p_0^{(r)}+p_0^{(l)}\right)+\sum_{n=1}^{\infty}\frac{2e^{-n\eta_0}}{1+e^{-2n\eta_0}}\left(p_n^{(r)}+p_n^{(l)}\right)$$
$$-\left(2\ln(2c)-\eta_0+\sum_{n=1}^{\infty}\frac{4}{n}\frac{e^{-2n\eta_0}}{1+e^{-2n\eta_0}}\right)\left(p_0^{(r)}-p_0^{(l)}\right)/(-\eta_0). \tag{52}$$

If the coefficients of $a_0^{(r)}$ and $a_0^{(l)}$ are equal to zero, i.e.

$$2\ln(2c)-\eta_0+\sum_{n=1}^{\infty}\frac{4}{n}\left(\frac{e^{-2n\eta_0}}{1+e^{-2n\eta_0}}\right)=0, \tag{53}$$

then the unknown Fourier coefficients, $a_0^{(r)}$ and $a_0^{(l)}$ cannot be determined. This parameter, $\eta_0=\eta_d$ satisfying Eq. (53) yields a degenerate scale.

### 2.4. Analytical derivation of the degenerate scale for the half-plane with a circular hole

For the half-plane problem subject to the special boundary condition, it would be transformed to an infinite plane problem by using the image method. In this subsection, we discuss the degenerate scale of the half-plane subject to the Dirichlet or the Neumann boundary condition. If the boundary condition at the boundary line for the half-plane is $\bar{u}(\mathbf{x})=0|_{\mathbf{x}\in B_\Gamma}$, then the anti-symmetric boundary conditions at the two circular boundaries satisfy

$$\bar{u}_r(\mathbf{x}_r)=-\bar{u}_l(\mathbf{x}_l),\ \mathbf{x}_r=(x_1,x_2)\in B_r\ and\ \mathbf{x}_l=(-x_1,x_2)\in B_l. \tag{54}$$

Based on the boundary condition in Eq. (54), Corfdir and Bonnet [23] and Chen [24] employed the Green's function as shown below:

$$U_D(\mathbf{s},\mathbf{x})=\ln|\mathbf{s}-\mathbf{x}|-\ln|\mathbf{s}^*-\mathbf{x}|, \tag{55}$$

where $\mathbf{s}=(s_1,s_2)$ and $\mathbf{s}^*=(-s_1,s_2)$. Based on Eqs. (8) and (11), the corresponding kernel function of Eq. (55) in terms of bipolar coordinates is expanded as:

$$U_D(\mathbf{s},\mathbf{x})=U(\mathbf{s},\mathbf{x})-U(\mathbf{s}^*,\mathbf{x})$$
$$=\begin{cases}-\eta_s-\sum_{n=1}^{\infty}\frac{1}{n}\left[\left(e^{-n(\eta_x-\eta_s)}-e^{-n(\eta_x+\eta_s)}\right)\cos\left[n(\xi_x-\xi_s)\right]\right],\\ \eta_x\geq\eta_s\geq 0,\\ -\eta_x-\sum_{n=1}^{\infty}\frac{1}{n}\left[\left(e^{-n(\eta_s-\eta_x)}-e^{-n(\eta_x+\eta_s)}\right)\cos\left[n(\xi_x-\xi_s)\right]\right],\\ \eta_s>\eta_x>0,\end{cases} \tag{56}$$

where $\mathbf{s}=(\eta_s,\xi_s)$ and $\mathbf{s}^*=(-\eta_s,\xi_s)$. According to Eqs. (6) and (14) and the Dirichlet boundary condition of Eq. (54), substitution of Eqs. (56), (39) and (41) into Eq. (7) yields

$$2\pi\eta_0a_0^{(r)}+\sum_{n=1}^{\infty}\frac{\pi}{n}\left(1-e^{-2n\eta_0}\right)\cos(n\xi_x)a_n^{(r)}+\sum_{n=1}^{\infty}\frac{\pi}{n}\left(1-e^{-2n\eta_0}\right)\sin(n\xi_x)b_n^{(r)}$$
$$=-2\pi p_0^{(r)}-\sum_{n=1}^{\infty}\pi\left(1+e^{-2n\eta_0}\right)\cos(n\xi_x)p_n^{(r)}-\sum_{n=1}^{\infty}\pi\left(1+e^{-2n\eta_0}\right)\sin(n\xi_x)q_n^{(r)}, \tag{57}$$

after collocating on the boundary points. By comparing with the coefficients of Fourier base in Eq. (57), the coefficients are obtained as shown below:

$$a_0^{(r)}=-\frac{1}{\eta_0}p_0^{(r)}, \tag{58}$$

$$a_n^{(r)}=-n\frac{1+e^{-2n\eta_0}}{1-e^{-2n\eta_0}}p_n^{(r)}, \tag{59}$$

$$b_n^{(r)}=-n\frac{1+e^{-2n\eta_0}}{1-e^{-2n\eta_0}}q_n^{(r)}. \tag{60}$$

Eqs. (58) and (60) indicate that a unique solution is obtained. The analytical solution corresponding to the homogeneous Dirichlet condition on the boundary line is expressed by

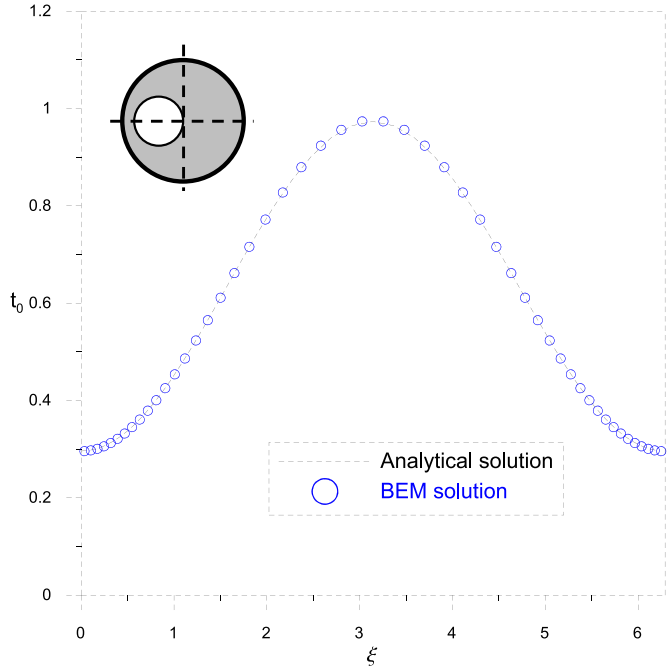


(a) Boundary flux along the outer boundary

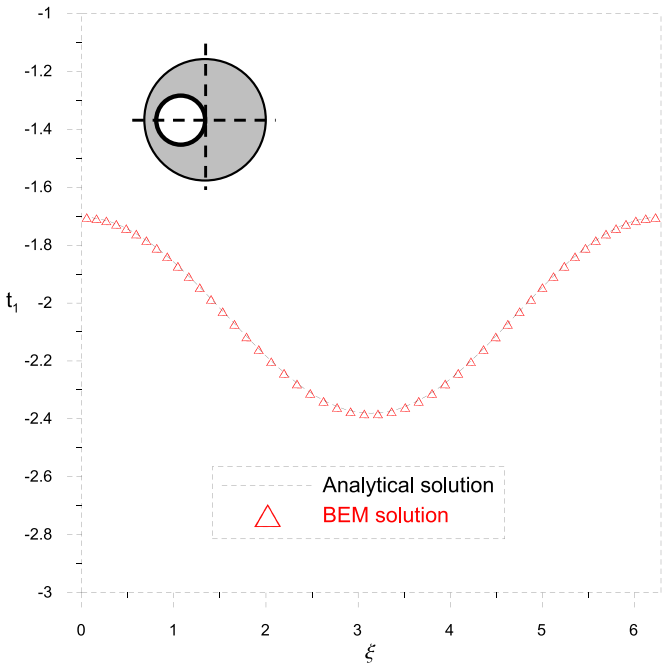


(b) Boundary flux along the inner boundary

**Fig. 4.** Boundary flux for the case of an ordinary scale of an eccentric annulus.

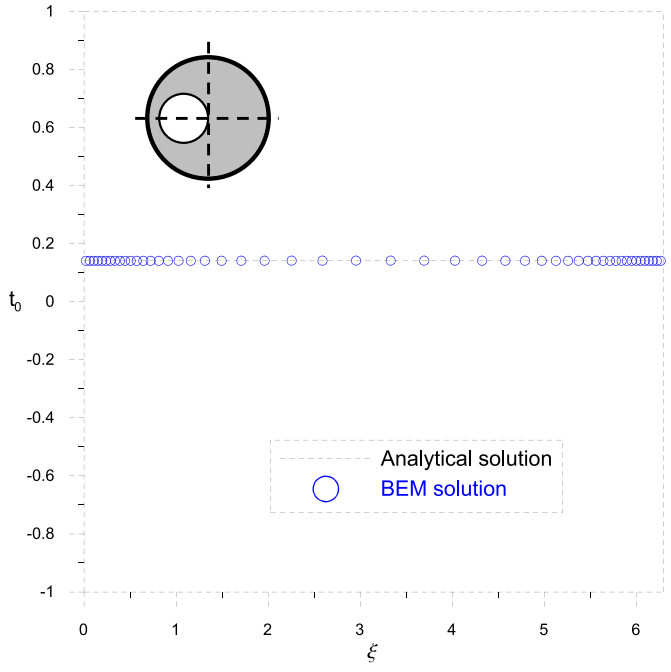


(a) Boundary flux along the outer boundary

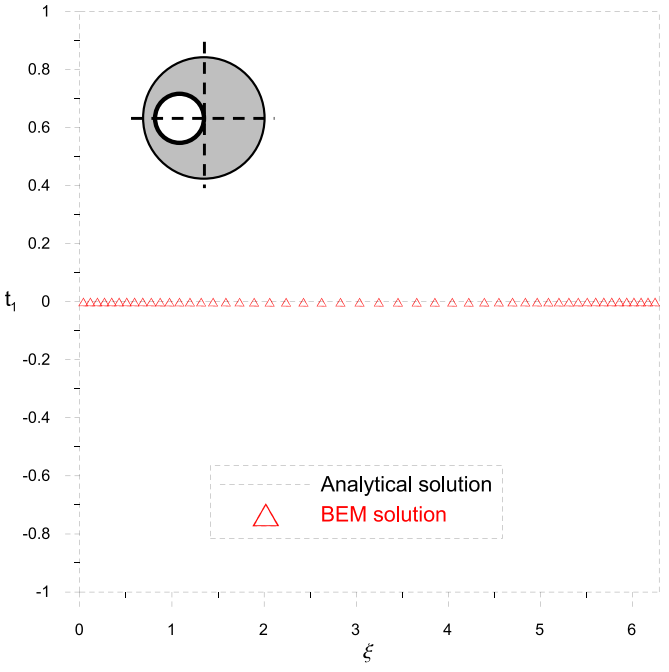


(b) Boundary flux along the inner boundary

**Fig. 5.** Boundary flux for the case of a degenerate scale of an eccentric annulus.

$$u(\mathbf{x}) = \frac{p_0^{(r)}}{\eta_0}\eta_x - \sum_{n=1}^{\infty}\left(\frac{e^{-n\eta_0}}{1-e^{-2n\eta_0}}p_n^{(r)}\sinh\left(n\eta_x\right)\cos\left(n\xi_x\right) + \frac{e^{-n\eta_0}}{1-e^{-2n\eta_0}}q_n^{(r)}\sinh\left(n\eta_x\right)\sin\left(n\xi_x\right)\right),\ \mathbf{x}\in D. \tag{61}$$

It is found that the space of solution does not have the constant term even though the constant term of boundary density, $a_0^{(r)}$, is not equal to zero. The reason is that the kernel function in Eq. (56) does not contain a constant term for the domain point. It is why Chen [24] explained that no degenerate scale occurs since the scaling factor disappears in the kernel function of Eq. (55) after scaling transformation. In other

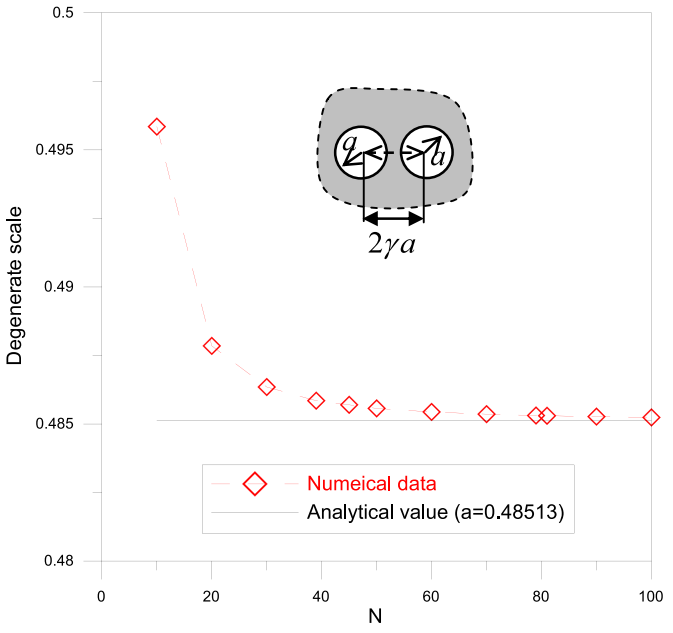


**Fig. 6.** Degenerate scale versus the number of boundary elements of each boundary for the case of the infinite plane with two identical circular holes ($\gamma = 2$).

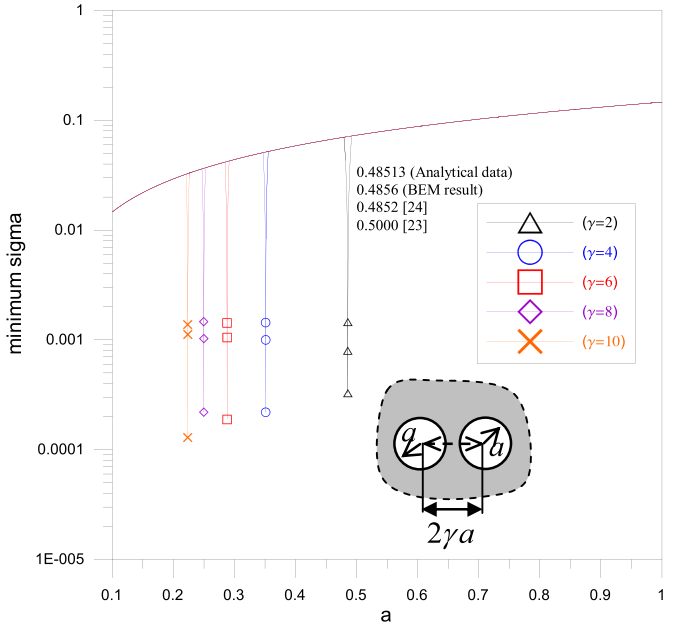


**Fig. 7.** Minimum singular value versus the radius for the case of the infinite plane with two identical circular holes.

words, there is no the degenerate scale for the Dirichlet condition on the boundary line of the half-plane if the employed kernel function is the Green's function of Eq. (55).

For the case of the boundary condition at the boundary line is $t(\mathbf{x}) = 0|_{\mathbf{x}\in B_\Gamma}$, the symmetric boundary conditions at the two circular boundaries satisfy

$$\bar{u}_r(\mathbf{x}_r) = \bar{u}_l(\mathbf{x}_l),\ \mathbf{x}_r = (x_1, x_2) \in B_r \text{ and } \mathbf{x}_l = (-x_1, x_2) \in B_l. \tag{62}$$

Based on the boundary condition in Eq. (62), the Green's function employed by Corfdir and Bonnet [23] and Chen [24] is

$$U_N(\mathbf{s}, \mathbf{x}) = \ln|\mathbf{s} - \mathbf{x}| + \ln|\mathbf{s}^* - \mathbf{x}|. \tag{63}$$

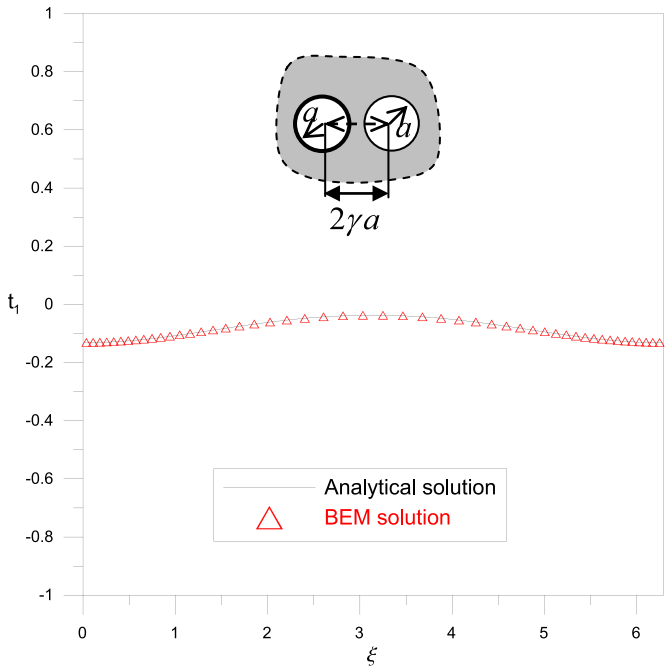


(a) Boundary flux along the left boundary

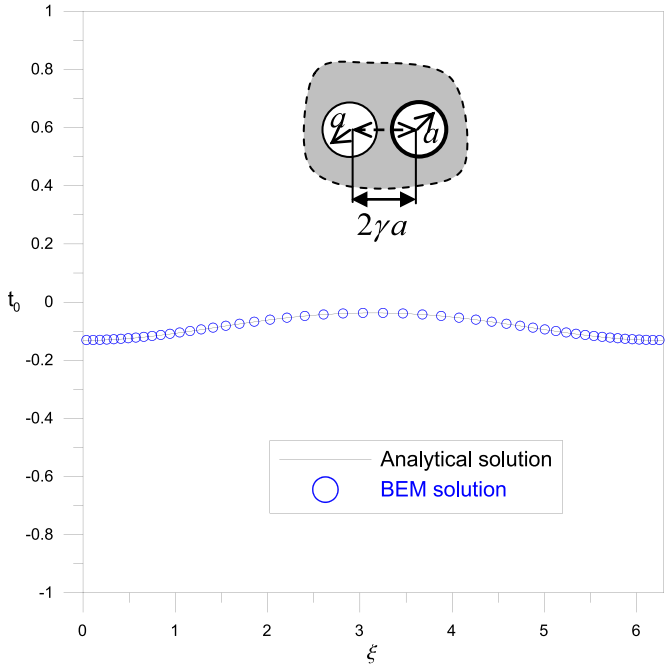


(b) Boundary flux along the right boundary

**Fig. 8.** Boundary flux for the case of a degenerate scale of the infinite plane with two identical circular holes.

Based on Eqs. (8) and (11), the corresponding kernel function of Eq. (63) is expanded as:

$$U_N(\mathbf{s}, \mathbf{x}) = U(\mathbf{s}, \mathbf{x}) + U(\mathbf{s}^*, \mathbf{x})$$
$$= \begin{cases} 2\ln(2c) - \eta_s - \sum_{n=1}^{\infty} \frac{1}{n}\left[\left(e^{-n(\eta_x-\eta_s)} + e^{-n(\eta_x+\eta_s)}\right)\cos\left[n(\xi_x-\xi_s)\right]\right. \\ \left. -2e^{-n\eta_x}\cos(n\xi_x) - 2e^{-n\eta_s}\cos(n\xi_s)\right],\ \eta_x \geq \eta_s \geq 0, \\ 2\ln(2c) - \eta_x - \sum_{n=1}^{\infty} \frac{1}{n}\left[\left(e^{-n(\eta_s-\eta_x)} + e^{-n(\eta_x+\eta_s)}\right)\cos\left[n(\xi_x-\xi_s)\right]\right. \\ \left. -2e^{-n\eta_x}\cos(n\xi_x) - 2e^{-n\eta_s}\cos(n\xi_s)\right],\ \eta_s > \eta_x > 0. \end{cases} \tag{64}$$

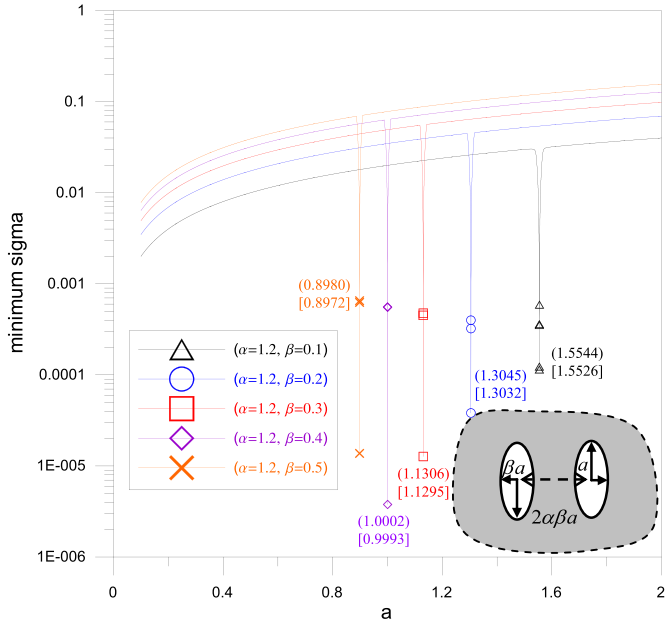


**Fig. 9.** Minimum singular value versus the length of the semi-major axis for $\alpha = 1.2$.

According to Eqs. (6) and (14) and the Neumann boundary condition of Eq. (62), substitution of Eqs. (64), (39) and (41) into Eq. (7) yields

$$
\begin{aligned}
&2\pi\left(2\ln(2c)-\eta_0\right)a_0^{(r)}-\sum_{n=1}^{\infty}\frac{\pi}{n}\left(1+e^{-2n\eta_0}\right)\cos(n\xi_x)a_n^{(r)}\\
&-\sum_{n=1}^{\infty}\frac{\pi}{n}\left(1+e^{-2n\eta_0}\right)\sin(n\xi_x)b_n^{(r)}\\
&+\sum_{n=1}^{\infty}\frac{4\pi}{n}e^{-n\eta_0}\cos(n\xi_x)a_0^{(r)}+\sum_{n=1}^{\infty}\frac{2\pi}{n}e^{-n\eta_0}a_n^{(r)}\\
&=2\pi p_0^{(r)}+\sum_{n=1}^{\infty}\pi\left(1-e^{-2n\eta_0}\right)\cos(n\xi_x)p_n^{(r)}\\
&+\sum_{n=1}^{\infty}\pi\left(1-e^{-2n\eta_0}\right)\sin(n\xi_x)q_n^{(r)}-\sum_{n=1}^{\infty}2\pi e^{-n\eta_0}p_n^{(r)},
\end{aligned}
\tag{65}
$$

after collocating on the boundary points. By comparing with the coefficients of Fourier base in Eq. (65), the coefficients could be obtained as shown below:

$$
\left(2\ln(2c)-\eta_0+\sum_{n=1}^{\infty}\frac{4}{n}\frac{e^{-2n\eta_0}}{1+e^{-2n\eta_0}}\right)a_0^{(r)}=p_0^{(r)}+\sum_{n=1}^{\infty}\frac{2e^{-2n\eta_0}}{1+e^{-2n\eta_0}}p_n^{(r)},
\tag{66}
$$

$$
a_n^{(r)}=\frac{4e^{-n\eta_0}}{1+e^{-2n\eta_0}}a_0^{(r)}-n\frac{1-e^{-2n\eta_0}}{1+e^{-2n\eta_0}}p_n^{(r)},
\tag{67}
$$

$$
b_n^{(r)}=-n\frac{1-e^{-2n\eta_0}}{1+e^{-2n\eta_0}}q_n^{(r)}.
\tag{68}
$$

If the variable, $\eta_0 = \eta_d$ satisfies Eq. (53), then Eq. (66) could be simplified to

$$
0\cdot a_0^{(r)}=p_0^{(r)}+\sum_{n=1}^{\infty}\frac{2e^{-2n\eta_0}}{1+e^{-2n\eta_0}}p_n^{(r)}.
\tag{69}
$$

According to the Fredholm alternative theorem, the degenerate scale of the half-plane problem may result in no solution ($p_0^{(r)}+\sum_{n=1}^{\infty}\frac{2e^{-n\eta_d}}{1+e^{-2n\eta_d}}p_n^{(r)}\neq 0$) or infinite solutions ($p_0^{(r)}+\sum_{n=1}^{\infty}\frac{2e^{-n\eta_d}}{1+e^{-2n\eta_d}}p_n^{(r)}=0$) corresponding to the Neumann condition on the boundary line.

Based on the above analytical derivation, the results agree with those in [23, 24]. However, some users of the BEM/BIEM may directly employ the fundamental solution for Laplace equation in Eq. (5) to deal with the half-plane problem even if they use the image method. According to the boundary condition of Eq. (54), Eqs. (51) and (52) are simplified to

$$
\begin{aligned}
&\left(2\ln(2c)-\eta_0+\sum_{n=1}^{\infty}\frac{4}{n}\frac{e^{-2n\eta_0}}{1+e^{-2n\eta_0}}\right)a_0^{(r)}\\
&=\left(2\ln(2c)-\eta_0+\sum_{n=1}^{\infty}\frac{4}{n}\frac{e^{-2n\eta_0}}{1+e^{-2n\eta_0}}\right)p_0^{(r)}/(-\eta_0),
\end{aligned}
\tag{70}
$$

$$
\begin{aligned}
&\left(2\ln(2c)-\eta_0+\sum_{n=1}^{\infty}\frac{4}{n}\frac{e^{-2n\eta_0}}{1+e^{-2n\eta_0}}\right)a_0^{(l)}\\
&=-\left(2\ln(2c)-\eta_0+\sum_{n=1}^{\infty}\frac{4}{n}\frac{e^{-2n\eta_0}}{1+e^{-2n\eta_0}}\right)p_0^{(r)}/(-\eta_0).
\end{aligned}
\tag{71}
$$

If the parameter, $\eta_0 = \eta_d$ satisfies Eq. (53), then

$$
0\cdot a_0^{(r)}=0
\tag{72}
$$

and

$$
0\cdot a_0^{(l)}=0.
\tag{73}
$$

According to the Fredholm alternative theorem, it would result in infinite solutions corresponding to the Dirichlet condition on the boundary line. For the Neumann boundary condition in Eq. (62), Eqs. (51) and (52) are simplified to

$$
\left(2\ln(2c)-\eta_0+\sum_{n=1}^{\infty}\frac{4}{n}\frac{e^{-2n\eta_0}}{1+e^{-2n\eta_0}}\right)a_0^{(r)}=p_0^{(r)}+\sum_{n=1}^{\infty}\frac{2e^{-n\eta_0}}{1+e^{-2n\eta_0}}p_n^{(r)}
\tag{74}
$$

$$
\left(2\ln(2c)-\eta_0+\sum_{n=1}^{\infty}\frac{4}{n}\frac{e^{-2n\eta_0}}{1+e^{-2n\eta_0}}\right)a_0^{(l)}=p_0^{(r)}+\sum_{n=1}^{\infty}\frac{2e^{-n\eta_0}}{1+e^{-2n\eta_0}}p_n^{(r)}.
\tag{75}
$$

If the parameter, $\eta_0 = \eta_d$ satisfies Eq. (53), then

$$
0\cdot a_0^{(r)}=p_0^{(r)}+\sum_{n=1}^{\infty}\frac{2e^{-n\eta_d}}{1+e^{-2n\eta_d}}p_n^{(r)}
\tag{76}
$$

and

$$
0\cdot a_0^{(l)}=p_0^{(r)}+\sum_{n=1}^{\infty}\frac{2e^{-n\eta_d}}{1+e^{-2n\eta_d}}p_n^{(r)}.
\tag{77}
$$

According to the Fredholm alternative theorem, the degenerate scale of the half-plane problem may result in no solution ($p_0^{(r)}+\sum_{n=1}^{\infty}\frac{2e^{-n\eta_d}}{1+e^{-2n\eta_d}}p_n^{(r)}\neq 0$) or infinite solutions ($p_0^{(r)}+\sum_{n=1}^{\infty}\frac{2e^{-n\eta_d}}{1+e^{-2n\eta_d}}p_n^{(r)}=0$) corresponding to the Neumann condition on the boundary line.

To the best of authors' knowledge, the degenerate scale parasitizes the kernel function. When the size of the domain is at the degenerate scale, the constant term cannot be represented by using the BEM/BIEM. In other words, the phenomenon of the degenerate scale depends upon the employed kernel function. The Green's function in Eq. (55) only presents the anti-symmetric response, since the weights of these two sources are opposite. Similarly, the Green's function of Eq. (63) for the Neumann boundary condition only presents the symmetric response. For the infinite plane with two identical circular holes subject to the anti-symmetric Dirichlet boundary conditions, the space of solution does not have the constant term. Therefore, the unique solution for the half-plane problem subject to the homogeneous Dirichlet boundary condition on the boundary line can be obtained by using Eq. (55). On the contrary, the space of solution may have a constant term for the symmetric Dirichlet boundary condition. When a degenerate scale occurs in the infinite plane with two identical circular holes, the coefficients of constant term could not be determined. In other words, the range of the response is deficient by a constant term when the real size is at a degenerate scale. This reason can explain why a degenerate scale may occur in a half-plane problem subject to the homogeneous Neumann boundary condition on the boundary line. When one employs the fundamental solution of the

**Table 2**
Relations between the kernel functions and the degenerate scale in half-plane problems.

| Kernel function | B.C. | |
|---|---|---|
| | Dirichlet B.C. | Neumann B.C. |
| Fundamental solution | $U(\mathbf{s},\mathbf{x})=\ln\lvert\mathbf{s}-\mathbf{x}\rvert$<br>Infinite solutions (Degenerate scale) | $U(\mathbf{s},\mathbf{x})=\ln\lvert\mathbf{s}-\mathbf{x}\rvert$<br>No solution or infinite solutions (Degenerate scale) |
| Green's function | $U_D(\mathbf{s},\mathbf{x})=\ln\lvert\mathbf{s}-\mathbf{x}\rvert-\ln\lvert\mathbf{s}^*-\mathbf{x}\rvert$<br>Unique solution (No degenerate scale) | $U_N(\mathbf{s},\mathbf{x})=\ln\lvert\mathbf{s}-\mathbf{x}\rvert+\ln\lvert\mathbf{s}^*-\mathbf{x}\rvert$<br>No solution or infinite solutions (Degenerate scale) |

**Table 3**
Modal participation factor for the infinite plane with two identical circular holes ($a=0.48557090999991$, $\gamma=2$).

| Boundary condition on the boundary line | Minimum singular value $\sigma_{100}$ | Modal participation factor $\gamma_{100}$ | Generalized force term for the minimum singular value $\beta_{100}$ |
|---|---|---|---|
| Dirichlet ($u(x)=0$) | $6.84077\times10^{-10}$ | $4.36168\times10^{-6}$ | 0 |
| Neumann ($t(x)=0$) | | $1.38381\times10^{10}$ | 9.46634 |

**Table 4**
Contour plots of the null field for the ordinary and degenerate scale of the eccentric annulus.

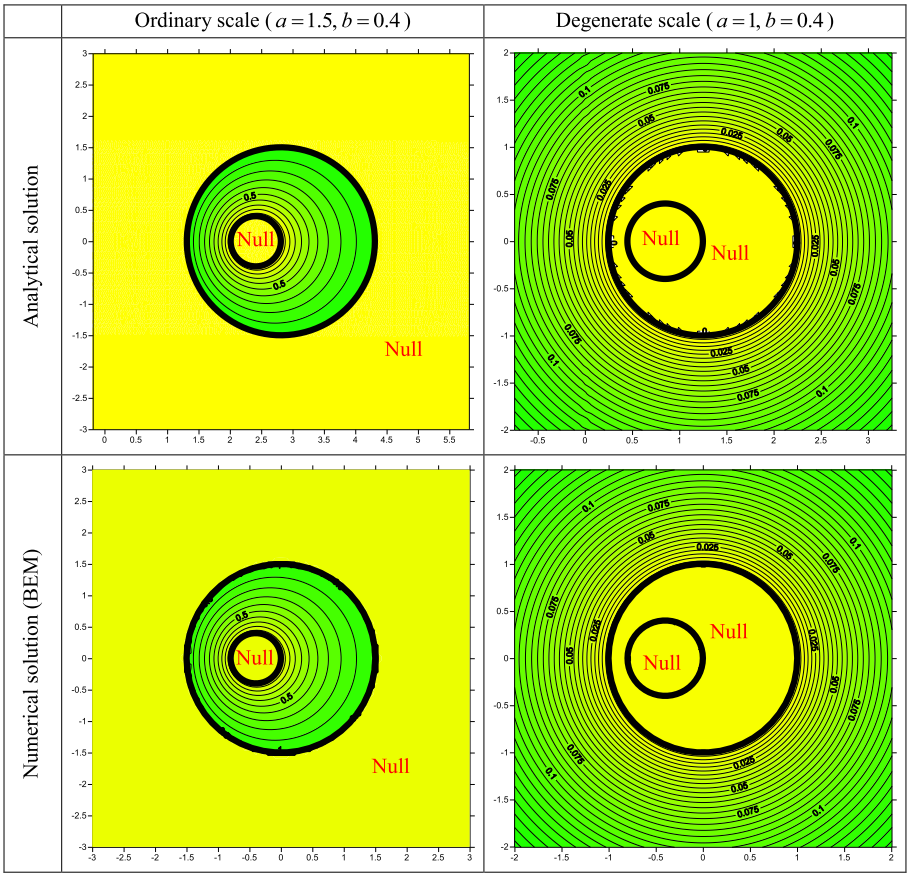


Laplace equation, ln*r*, the degenerate scale may exist in both the above two kinds of boundary conditions. The comparison is given in Table 2.

In addition, we can use the concept of modal participation factor to explain the outcome of Corfdir and Bonnet [23] and Chen [24]. In the discrete system, we have

$$[U]\{t\}=[T]\{u\}, \tag{78}$$

where $[U]$ and $[T]$ are the influence matrices by using the fundamental solution of the Laplace equation, ln*r*, $\{u\}$ and $\{t\}$ are the boundary densities. By using the singular value decomposition, $[U]$ can be expressed by

$$[U]=[\Phi][\Sigma][\Psi]^T, \tag{79}$$

where $[\Sigma]$ is a diagonal matrix corresponding to singular values of $[U]$, $[\Phi]$ and $[\Psi]$ are left and right singular matrices. The unknown boundary data can be expressed by

$$\{t\}=[\Psi]\{\gamma\}. \tag{80}$$

The right-hand side of Eq. (78) is rewritten as

$$[T]\{u\}=\{b\}=[\Phi]\{\beta\}, \tag{81}$$

where $\{\beta\}$ means the generalized forcing term. Substituting Eqs. (79)–(81) into Eq. (78), we obtain

$$[\Sigma]\{\gamma\}=\{\beta\}, \tag{82}$$

where $\sigma_i\gamma_i=\beta_i$, $i=1, 2, \ldots, N$, and $\gamma_i$ is the $i$th modal participation factor corresponding to the $i$th singular value $\sigma_i$. For the homogeneous Dirich-

**Table 5**
3-D plots of the null field for the ordinary and degenerate scale of the eccentric annulus.

| | Ordinary scale | Degenerate scale |
|---|---|---|
| Analytical solution | 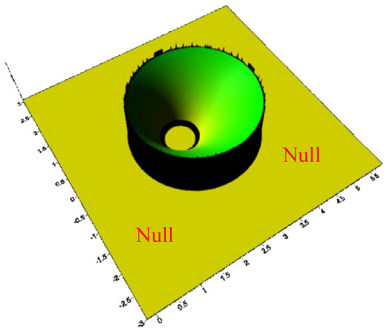  | 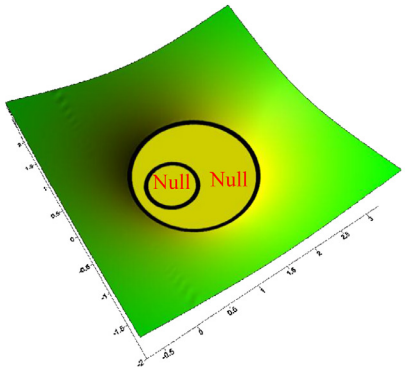  |
| Numerical solution (BEM) | 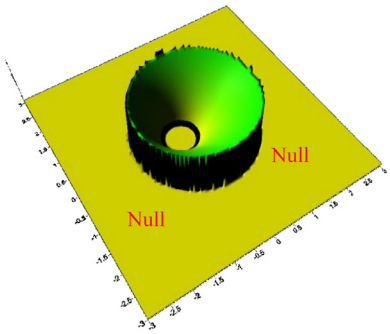  | 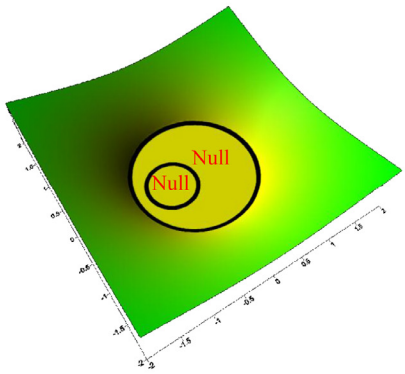  |

let and Neumann boundary condition on the boundary line, the modal participation factors are both addressed in Table 3. This explained why the solution for the infinite plane problem subject to the homogeneous Dirichlet boundary condition on the boundary line obtained by the BEM is acceptable, but one of the Neumann condition is not.

## 3. Numerical examples and discussions

In this section, we employ the BEM to numerically verify the degenerate scale of two cases. One is an eccentric annulus and the other is an infinite plane containing two holes. First, the null field and solution space of the ordinary and degenerate scales for the eccentric annulus were addressed, respectively. In addition, degenerate scales of the infinite plane containing circular, elliptical and rectangular holes are considered. The distance between the two centers of the holes is denoted as $d_e$ for the case of infinite domain. The analytical derivation and the BEM implementations are addressed as follows.

### 3.1. Null field and nonzero field of an eccentric annulus

The degenerate scale occurs due to the kernel function of the mathematical model rather than the real physical behavior. In the discrete system, the degenerate scale results in the numerical instability. The null field and nonzero field of the solution representation for the degenerate scale are studied. First, the solution representation for an ordinary scale of the eccentric annulus is addressed. The radii of the outer and inner circles are 1.5 and 0.4, respectively. The distance between the two centers is 0.4. The given boundary conditions are $u_0(\mathbf{x})=1,\ \mathbf{x}\in B_0$ and $u_1(\mathbf{x})=0,\ \mathbf{x}\in B_1$. Based on the above given boundary conditions and comparing with the coefficients in Eqs. (29) and (30), we obtain the boundary data of an eccentric annulus

$$t_0(\mathbf{s})=\left(\frac{\cosh\eta_0-\cos\xi_s}{c}\right)\left(\frac{1}{\eta_1-\eta_0}\right),\ \mathbf{s}\in B_0 \text{ and } 0\le\xi_s\le 2\pi, \tag{83}$$

$$t_1(\mathbf{s})=-\left(\frac{\cosh\eta_0-\cos\xi_s}{c}\right)\left(\frac{1}{\eta_1-\eta_0}\right),\ \mathbf{s}\in B_1 \text{ and } 0\le\xi_s\le 2\pi, \tag{84}$$

as shown in Fig. 4(a) and (b), respectively. The nonzero interior field and the null exterior field for the ordinary scale are, respectively, expressed by

$$u(\mathbf{x})=1-\frac{\eta-\eta_0}{\eta_1-\eta_0},\ \mathbf{x}\in D,\quad \text{interior field} \tag{85}$$

$$u(\mathbf{x})=0,\ \mathbf{x}\in D^c,\ \text{null field}. \tag{86}$$

The contour plot and 3-D plot of the solution representation are shown in Tables 4 and 5.

For the degenerate scale, the radii of the outer and inner circles are 1 and 0.4, respectively. The distance between the two centers is 0.4. The Dirichlet boundary conditions are specified to be trivial to introduce nontrivial boundary flux. Then, the corresponding nontrivial boundary data are obtained

$$t_0(\mathbf{s})=-\left(\frac{\cosh\eta_0-\cos\xi_s}{c}\right)\left[1+\sum_{n=1}^{\infty}2e^{-n\eta_0}\cos(n\xi_s)\right]a_0^{(0)},\quad \mathbf{s}\in B_0 \text{ and } 0\le\xi_s\le 2\pi, \tag{87}$$

$$t_1(\mathbf{s})=0,\ \mathbf{s}\in B_1 \text{ and } 0\le\xi_s\le 2\pi, \tag{88}$$

where the size of $B_0$ is the degenerate scale. Boundary flux of inner and outer boundaries, are respectively, shown in Fig. 5(a) and (b). Based on the generating function related to hyperbolic and trigonometric functions, we have

**Table 6**
Degenerate scales for the infinite plane with two identical circular holes.

| Method | $\gamma$ | | | | | |
|---|---|---|---|---|---|---|
| | 2 | 4 | 6 | 8 | 10 | ∞ |
| Present (Analytical data) | 0.48513 | 0.35082 | 0.28768 | 0.24951 | 0.22332 | $e^{-\eta_d/2} \approx 0$ |
| BEM (Numerical data) ($N = 50$) | 0.4856 | 0.3511 | 0.2879 | 0.2497 | 0.2235 | 0.02238 ($\gamma = 2000$) |
| Chen [24] (Null field BIE) | 0.4852 | 0.3509 | 0.2877 | 0.2496 | 0.2234 | NA |
| Corfder and Bonnet [23] (Asymptotic result) | 0.5000 | 0.3536 | 0.2887 | 0.2500 | 0.2236 | $e^{-\eta_d/2} \approx 0$ |

Note: $N$ is the number of elements for each boundary.

**Table 7**
Geometry parameter of degenerate scale in terms of bipolar coordinates for the infinite plane with two identical circular holes.

| $\gamma$ | 2 | 4 | 6 | 8 | 10 | ∞ |
|---|---|---|---|---|---|---|
| $a_d$ | 0.48513 | 0.35082 | 0.28768 | 0.24951 | 0.22332 | $e^{-\eta_d/2}$ |
| $\eta_d$ | 1.31696 | 2.06344 | 2.47789 | 2.76866 | 2.99322 | $\cosh^{-1}(\gamma)$ |
| $c$ | 0.84027 | 1.35874 | 1.70193 | 1.98045 | 2.22208 | $e^{\eta_d/2}$ |

$$1 + \sum_{n=1}^{\infty} 2e^{-n\eta_0}\cos(n\xi_s) = \frac{\sinh\eta_0}{\cosh\eta_0 - \cos\xi_s}. \tag{89}$$

Eq. (87) is rewritten as

$$t_0(\mathbf{s}) = -\frac{1}{a_d}a_0^{(0)} = -a_0^{(0)}, \ \mathbf{s} \in B_0 \text{ and } 0 \le \xi_s \le 2\pi, \tag{90}$$

after considering Eq. (24). Then, the nonzero exterior field and null interior field for the eccentric annulus with a degenerate scale are expressed by

$$u(\mathbf{x}) = \left(\ln(2c) - \eta_d + \sum_{n=1}^{\infty}\frac{1}{n}e^{-2n\eta_d}\right)a_0^{(0)} = 0,$$
$$\mathbf{x} \in D, \text{ for the interior field,} \tag{91}$$

$$u(\mathbf{x}) = \begin{cases} 0, & \eta_x \ge \eta_d \\ \left[(\eta_d - \eta_x) - \sum_{n=1}^{\infty}\frac{1}{n}\left(e^{-2n\eta_d + n\eta_x} - e^{-n\eta_x}\right)\cos(n\xi_x)\right]a_0^{(0)}, & \eta_x < \eta_d \end{cases},$$
$$\mathbf{x} \in D^c, \text{ for the exterior field,} \tag{92}$$

where $a_0^{(0)}$ is an arbitrarily real-valued constant. Here, we can obtain $a_0^{(0)} = 0.141421266$ according to the numerical result of BEM implementation. The contour plot and 3-D plot of the solution representation are shown in Tables 4 and 5. If the size of the boundary shape is a degenerate scale, the given homogeneous Dirichlet boundary conditions result

**Table 8**
Contour plots and 3D plots for the degenerate scale of the infinite plane with two identical circular holes.

| | Degenerate scale (Contour plot) | Degenerate scale (3D plot) |
|---|---|---|
| Analytical solution | 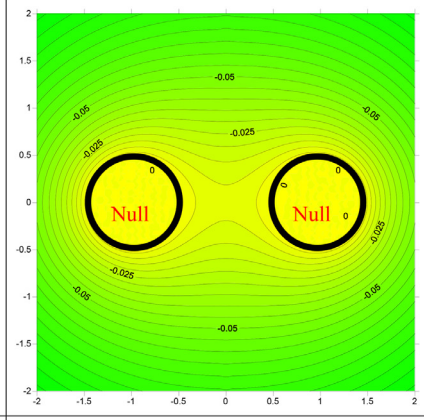 | 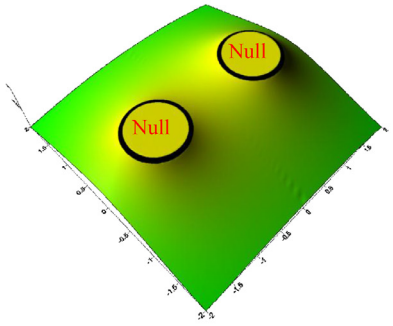 |
| Numerical solution (BEM) | 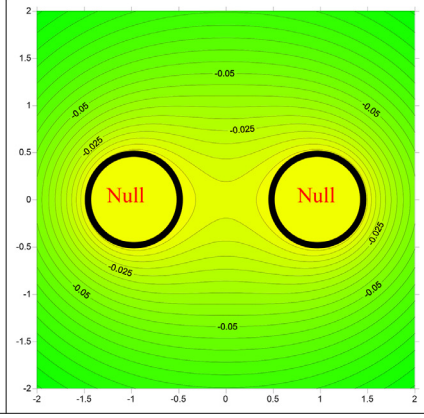 | 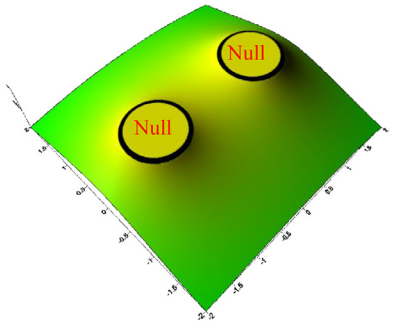 |

**Table 9**
Contour plots for the ordinary scale of the infinite plane with two identical circular holes.

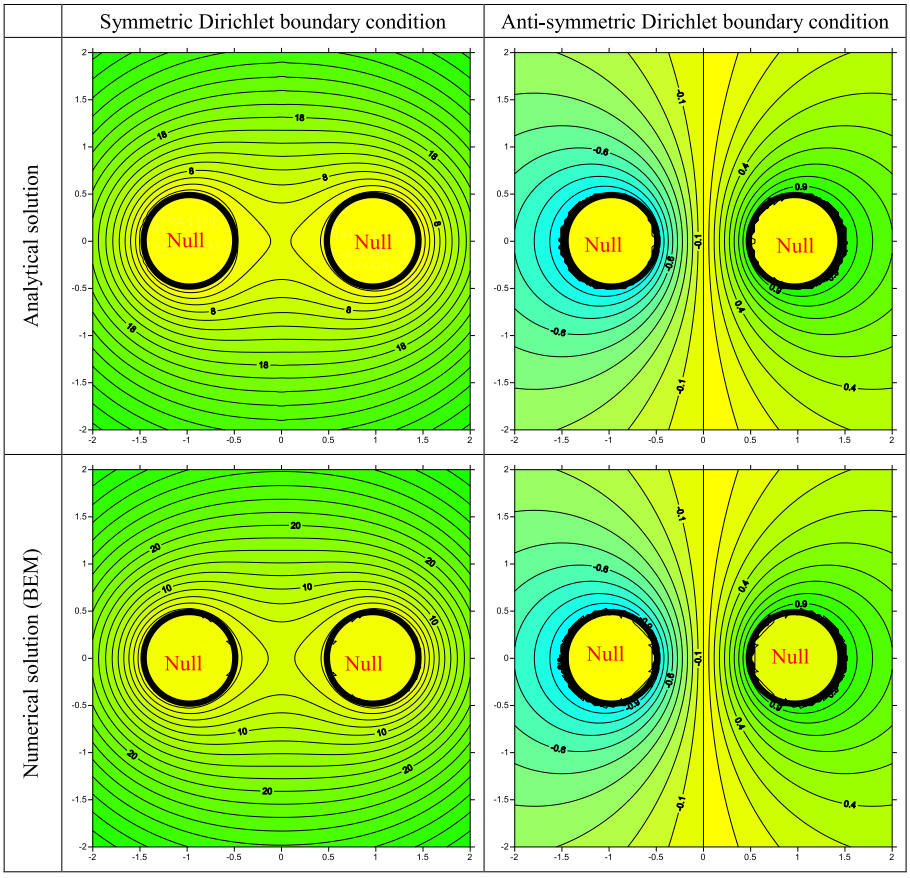


in non-trivial boundary flux. Owing to the non-trivial boundary flux, it is found that the field in the domain is null. In the complementary domain outside the outer circular boundary, it is a nonzero field.

### 3.2. An infinite plane containing two identical holes

In this subsection, the BEM was employed to verify the degenerate scale of the infinite plane containing holes. For the circular case, the distance between centers of the two circles is defined by

$$2d_e = 2\gamma a = 2c\frac{\cosh\eta_0}{\sinh\eta_0}, \tag{93}$$

where $\gamma$ is the geometric parameter. If the size of the circular hole is a degenerate scale, then the influence matrix constructed by $U(\mathbf{s}, \mathbf{x})$ of the BEM is singular. In other words, the minimum singular value is equal to zero. While $\gamma = 2$, the numerical result converges to the analytical result as shown in Fig. 6. According to the minimum singular value, the degenerate scale versus the parameter, $\gamma$, is obtained as shown in Fig. 7 and Table 6. The corresponding analytical results are shown in Table 7. Good agreement between analytical and numerical results is made. For the limiting case, $\gamma = \cosh\eta_0 \to \infty$, it means that $e^{\eta_0} \to \infty$. Eq. (53) can be rewritten as

$$2\ln(2c) - \eta_0 \approx 0. \tag{94}$$

In other words, the degenerate scale $a_d$ can be expressed by

$$a_d = \frac{c}{\sinh\eta_d} = \frac{2c}{e^{\eta_d} - e^{-\eta_d}} \approx e^{-\eta_d/2}. \tag{95}$$

This agrees with the asymptotic solution [23] for the degenerate scale as shown below,

$$a_d \approx \sqrt{\frac{1}{2\gamma}} = \sqrt{\frac{1}{e^{\eta_d} + e^{-\eta_d}}} \approx e^{-\eta_d/2}. \tag{96}$$

These results are summarized in Tables 6 and 7.

For the degenerate scale, the radii of the right and left circular holes are both equal to 0.485571 while $\gamma = 2$. Although the homogeneous Dirichlet boundary condition is given, the corresponding nontrivial boundary fluxes are

$$t_l(\mathbf{s}) = -\frac{\cosh(-\eta_d) - \cos\xi_s}{c}\left[1 + \sum_{n=1}^{\infty}\frac{4e^{-n\eta_d}}{1+e^{-2n\eta_d}}\cos(n\xi_s)\right]a_0^{(r)}, \quad \mathbf{s} \in B_l \text{ and } 0 \le \xi_s \le 2\pi, \tag{97}$$

$$t_r(\mathbf{s}) = -\frac{\cosh\eta_d - \cos\xi_s}{c}\left[1 + \sum_{n=1}^{\infty}\frac{4e^{-n\eta_d}}{1+e^{-2n\eta_d}}\cos(n\xi_s)\right]a_0^{(r)}, \quad \mathbf{s} \in B_r \text{ and } 0 \le \xi_s \le 2\pi, \tag{98}$$

as shown in Fig. 8. Then, the nonzero field in the domain and the null field in the complementary domain are, respectively, expressed by

$$u(\mathbf{x}) = \begin{cases} -\left((\eta_d - \eta_x) - \sum_{n=1}^{\infty}\frac{2}{n}\left((e^{n\eta_x} + e^{-n\eta_x})\frac{e^{-2n\eta_d}}{1+e^{-2n\eta_d}} - e^{-n\eta_x}\right)\cos(n\xi_x)\right)a_0^{(r)}, \\ \eta_x \ge 0, \\ -\left((\eta_d + \eta_x) - \sum_{n=1}^{\infty}\frac{2}{n}\left((e^{n\eta_x} + e^{-n\eta_x})\frac{e^{-2n\eta_d}}{1+e^{-2n\eta_d}} - e^{n\eta_x}\right)\cos(n\xi_x)\right)a_0^{(r)}, \\ \eta_x < 0, \end{cases} \quad \mathbf{x} \in D, \tag{99}$$

$$u(\mathbf{x}) = 0, \ \mathbf{x} \in D^c, \tag{100}$$

where $a_0^{(r)}$ is an arbitrarily real-valued constant . Here, we obtain $a_0^{(r)} = 0.046329$ according to the numerical result of BEM implementation. The

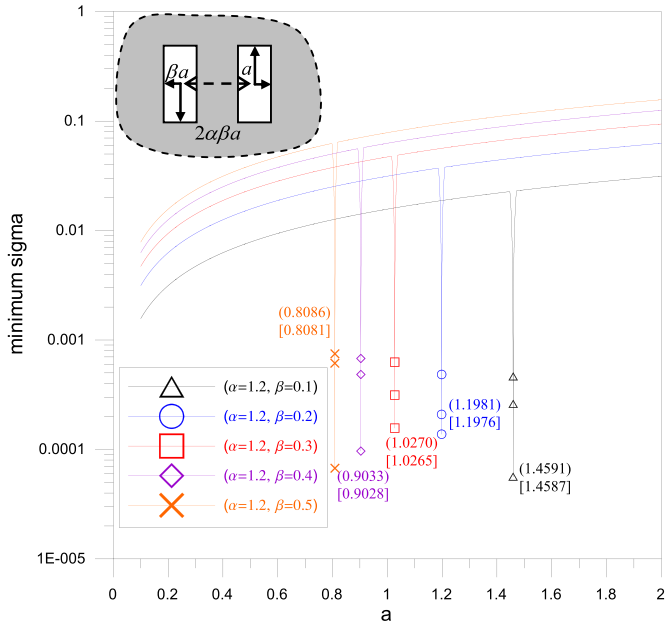


**Fig. 10.** Minimum singular value versus the length of the rectangle for $\alpha = 1.2$. (The values inside the parentheses() and the square bracket [] denote the analytical value and Chen's results [24],-respectively.)

**Table 10**
Degenerate scales for the infinite plane with two identical elliptical holes ($\alpha = 1.2$).

| | $\beta$ | | | | |
|---|---|---|---|---|---|
| Method | 0.1 | 0.2 | 0.3 | 0.4 | 0.5 |
| BEM ($N = 50$) | 1.5544 | 1.3045 | 1.1306 | 1.0002 | 0.8980 |
| Chen [24] | 1.5526 | 1.3032 | 1.1295 | 0.9993 | 0.8972 |

Note: $N$ is the number of boundary elements for each ellipse.

**Table 11**
Degenerate scales for the infinite plane with two identical rectangular holes ($\alpha = 1.2$).

| | $\beta$ | | | | |
|---|---|---|---|---|---|
| Method | 0.1 | 0.2 | 0.3 | 0.4 | 0.5 |
| BEM ($N = 60$) | 1.4591 | 1.1981 | 1.0270 | 0.9033 | 0.8086 |
| Chen [24] | 1.4587 | 1.1976 | 1.0265 | 0.9028 | 0.8081 |

Note: $N$ is the number of boundary elements for each rectangle.

contour plot and 3-D plot for the case of degenerate scale are shown in Table 8. If the size of the boundary shape is a degenerate scale, the given homogeneous Dirichlet boundary conditions result in non-trivial boundary flux. Owing to the non-trivial boundary flux, it is found that the field in the domain is a nonzero field while a null field for a complementary domain.

For the ordinary scale, the radii of the right and left circular holes are both equal to 0.5 while $\gamma = 2$. The symmetric ($u_r(\mathbf{x}) = 1,\ \mathbf{x} \in B_r$ and $u_l(\mathbf{x}) = 1,\ \mathbf{x} \in B_l$) and anti-symmetric ($u_r(\mathbf{x}) = 1,\ \mathbf{x} \in B_r$ and $u_l(\mathbf{x}) = -1,\ \mathbf{x} \in B_l$) Dirichlet boundary conditions are both considered. The contour plots of the solution representation are shown in Table 9.

In addition, the elliptical and rectangular holes are also considered in the BEM implementation. The geometric parameters are shown in Fig. 3(d) and (e). According to the minimum singular value, the degenerate scale versus the geometric parameter, $\beta$, is obtained as shown in Figs. 9 and 10. The numerical results agree well with Chen's results [24] as shown in Tables 10 and 11. Since degenerate kernel is not available for bi-elliptical or bi-rectangular coordinates, no exact solution is compared with. The main point to provide above two noncircular cases is showing that two cavities of arbitrary shape in the infinite domain also have degenerate scales.

## 4. Conclusions

In this paper, the degenerate kernel for expressing the closed-form fundamental solution in terms of bipolar coordinates was employed to analytically study the degenerate scale of a circular domain, eccentric annulus and infinite plane with two identical circular cavities. The degenerate scale of a circular case was revisited by using the degenerate kernel in the bipolar coordinates. It was theoretically proved that the radius of the outer circle dominates the degenerate scale for the eccentric annulus. An analytical formula of degenerate scale for the infinite plane with two identical circular boundaries was also derived at the first time. Numerical examples by using the boundary element method were also demonstrated and compared well with the analytical solution. In addition, null fields for ordinary and degenerate scales were also addressed.

## Acknowledgment

Financial supports from the Ministry of Science and Technology under Grant No. MOST-103-2221-E-019-012-MY3, MOST-105-2811-E-019-001, MOST-105-2221-E-019-004 and MOST-106-2221-E-019-009-MY3 for National Taiwan Ocean University are gratefully acknowledged.

## References

[1] Jaswon MA, Symm GT. Integral equation methods in potential theory and elastostatics. New York: Academic Press; 1977.
[2] Rumely RS. Capacity theory on algebraic curves, 1378. Berlin: Springer-Verlag; 1989.
[3] Christiansen S. Detecting non-uniqueness of solutions to biharmonic integral equations through SVD. J Comput Appl Math 2001;134:23–35.
[4] Yan Y, Sloan IH. On integral equations of the first kind with logarithmic kernels. J Integr Equ Appl 1988;1:945–75.
[5] Chen YZ, Wang ZX, Lin XY. The degenerate scale problem for the Laplace equation and plane elasticity in a multiply connected region with an outer circular boundary. Int J Solids Struct 2009;46(13):2605–10.
[6] Kuo SR, Chen JT, Lee JW, Chen YW. Analytical derivation and numerical experiments of degenerate scale for regular N-gon domains in BEM. Appl Math Comput 2013;219:5668–83.
[7] Vodička R, Petrik M. Degenerate scales for boundary value problems in anisotropic elasticity. Int J Solids Struct 2015;52:209–19.
[8] Chen YZ, Lin XY, Wang ZX. Evaluation of the degenerate scale for BIE in plane elasticity and antiplane elasticity by using conformal mapping. Eng Anal Bound Elem 2009;33:147–58.
[9] Landkof NS. Foundations of modern potential theory. Berlin: Springer-Verlag; 1972.
[10] Dijkstra W. Condition numbers in the boundary element method: shape and solvability. (Ph.D Dissertation), Eindhoven University of Technology, Netherlands, 2008.
[11] Kuo SR, Chen JT, Kao SK. Linkage between the unit logarithmic capacity in the theory of complex variables and the degenerate scale in the BEM/BIEMs. Appl Math Lett 2016;29(6):929–38.
[12] Chen JT, Lin JH, Kuo SR, Chiu YP. Analytical study and numerical experiments for degenerate scale problems in boundary element method using degenerate kernels and circulants. Eng Anal Bound Elem 2001;25:819–28.
[13] Chen JT, Shen WC. Degenerate scale for multiply connected Laplace problems. Mech Res Commun 2007;34:69–77.
[14] He WJ, Ding HJ, Hu HC. Degenerate scales and boundary element analysis of two dimensional potential and elasticity problems. Comput Struct 1996;60:155–8.
[15] Liu PLF, Lean MH. A note on–contour in the integral equation formulation for a multi-connected region. In: Grilli S, Brebbia CA, Cheng AH-D, editors. Computational engineering with boundary elements vol. 1: fluid and potential problems. Boston:: Computational mechanics Publications; 1990. p. 295–302.
[16] Chen JT, Kuo SR, Lin JH. Analytical study and numerical experiments for degenerate scale problems in the boundary element method for two-dimensional elasticity. Int J Numer Methods Eng 2002;54:1669–81.
[17] Chen YZ, Wang ZX. Boundary integral equation method for periodic dissimilar elastic inclusions in an infinite plate. Appl Math Comput 2012;218:8578–91.
[18] Chen YZ. Numerical solution for degenerate scale problem arising from multiple rigid lines in plane elasticity. Appl Math Comput 2011;218:96–106.
[19] Chen YZ, Lin XY, Wang ZX. A semi-analytic solution for multiple curved cracks emanating from circular hole using singular integral equation. Appl Math Comput 2009;213:389–404.
[20] Chen JT, Wu CS, Chen KH, Lee YT. Degenerate scale for analysis of circular plate using the boundary integral equations and boundary element method. Comput Mech 2006;38:33–49.
[21] Hille E. Analytical function theory, vol. II. Boston:: Ginn and Company; 1962.

[22] Yan Y, Sloan IH. On integral equations of the first kind with logarithmic kernels. J Integr Equ Appl 1988;1:945–75.
[23] Corfdir A, Bonnet G. Degenerate scale for the Laplace problem in the half plane; approximate logarithmic capacity for two distant boundaries. Eng Anal Bound Elem 2014;37:836–41.
[24] Chen YZ. Numerical solution for the degenerate scale in 2D Laplace equation for notch in half-plane using null field BIE. Eng Anal Bound Elem 2016;70:126–33.
[25] Chen JT, Lin SR, Chen KH. Degenerate scale problem when solving Laplace's equation by BEM and its treatment. Int J Numer Methods Eng 2005;62:233–61.
[26] Chen JT, Lee YT, Kuo SR, Chen YW. Analytical derivation and numerical experiments of degenerate scale for an ellipse in BEM. Eng Anal Bound Elem 2012;36:1397–405.
[27] Chen JT, Lee JW, Chen IL, Kuo PS. On the null and nonzero fields for true and spurious eigenvalues of annular and confocal elliptical membranes. Eng Anal Bound Elem 2013;37:42–59.
[28] Kane JH. Boundary element analysis in engineering continuum mechanics. New Jersey: Prentice-Hall; 1994.
[29] Chen JT, Shen WC, Wu AC. Null-field integral equations for stress field around circular holes under antiplane shear. Eng Anal Bound Elem 2006;30(3):205–17.
[30] Morse P, Feshbach H. Method of theoretical physics. New York: McGraw-Hill; 1953.